

POLITECNICO DI TORINO

Master's Degree in Automotive Engineering



**Politecnico
di Torino**

Master's Degree Thesis

**Lateral Tire Model Parameter Estimation
Using Normalised Real Test Drive
Manoeuvres**

Supervisors

Prof. Andrea TONOLI

Prof. Alessandro VIGLIANI

Candidate

Alessandro SCURTI

March 2025

Summary

The work focuses on the lateral tire forces during cornering manoeuvres. The topic concerns the estimation of tire parameters with real manoeuvres on the track with a Formula Student car. An introduction is given to the current state of the art in tire ground contact force measurement techniques. This is followed by the description of the tire behaviour in a race car and the definition of the Pacejka Magic formula. The organisation and analysis of the track tests are reported. Fitting algorithms are developed to estimate tire parameters. The results are then verified by simulations on the team's LapTime Simulator. As a further step, the design of an Extended Kalman Filter is explained. Finally, a comparison is made with the laboratory test of FSAE Tire Testing Consortium data. The project is developed at the RWTH University of Aachen (Germany) in the Formula Student Team Ecurie Aix.

Acknowledgements

Al mio papà

Table of Contents

List of Figures	VII
1 Introduction	1
1.1 Formula Student Competition	1
1.1.1 RWTH Ecurie Aix	2
1.1.2 Tyre impact on Formula Student	3
1.1.3 Equipment and Sensors	3
2 State of art	5
2.1 Researches on sensors	5
2.2 Estimation methodologies	7
2.2.1 Control system technologies, focus on EKF	7
3 Tire Behavior	10
3.1 Normal Force F_z : load sensitivity	12
3.2 Inclination angle or Camber angle γ	13
3.3 Pressure	14
3.4 Temperature	15
4 Pacejka Magic Formula	16
5 Laptime Simulator	19
5.1 Logged data as input	24
5.2 Vehicle model	26
6 Track tests	29
6.1 Manoeuvres for testing	29
6.2 Analysis of logged data	35
7 Estimation of tire modelling parameters	40
7.1 Selection of data	40
7.1.1 Force evaluation	43

7.2	Tyre models	44
7.2.1	Simplified Pacejka	44
7.2.2	Normal loads	44
7.2.3	Pacejka with Fz	46
7.2.4	Heuristic approach Kiencke and Nielsen	46
7.3	Fitting procedures	49
7.3.1	Levenberg-Marquardt algorithm	49
7.3.2	Genetic Algorithm	51
8	Results	53
8.1	Curve Fitter with LMA	53
8.2	Lateral force characteristic $F_y(\alpha)$	54
8.3	Improvements on the model $F_y(\alpha, F_z)$	56
8.4	Simulink results	59
8.5	Extended Kalman Filter design	61
9	Tire Testing Consortium Data	69
9.1	What is the TTC	69
9.2	Laboratory data characteristics	70
9.3	Comparison	72
10	Conclusions	75
	Bibliography	78

List of Figures

2.1	WFT Megaone from Bota Systems	6
2.2	Strain gauge on a suspension arm	6
2.3	Intelligent tire, accelerometer in the wheel	6
2.4	Graphical scheme of the procedure adopted to estimate tire model parameters	8
3.1	Deformation of the footprint and distribution of forces over the contact patch	11
3.2	Side lateral force vs slip angle	12
3.3	Effect of Fz on Fy vs slip angle [7]	13
3.4	Camber effect on lateral force and roll-off [6]	14
4.1	Sensitivity analysis of the Pacejka parameters B,C,D,E	17
5.1	Laptime simulator loop	20
5.2	Example of aerodynamic 4D LUT for C_l evaluation	21
5.3	Figure output of LapSim simulation. Car data from eax02 on Autocross of FSG 2023	23
5.4	Trajectory analysis of the LapSim simulation. Car data from eax02 on Autocross of FSG 2023	24
5.5	Overview of Thesis simulink model	25
5.6	a_x and a_y equations in Simulink	27
5.7	$\dot{\psi}$ equation in Simulink	28
6.1	Matlab plot for the sinusoidal sweep steering audio	31
6.2	Aldenhoven testing area	32
6.3	Ramp steer at 100 km/h determination of the limit of the linear range of the car, paper [10]	33
6.4	Experimental ramp data to determine the limit of the linear range of the car	33
6.5	Ramp steer 30 km/h	35
6.6	Sinusoidal sweep steer 30 km/h	35

6.7	Hysteresis of lateral force in sweep sinusoidal maneuver	37
6.8	lateral acceleration and steering angle in sweep sinusoidal maneuver	37
6.9	lateral force reduction in amplitude at high frequency in sweep sinusoidal maneuver	38
6.10	Ramp steering steering angle versus time, right turn	39
6.11	Ramp steering steering angle versus time, left turn	39
7.1	Ramp steering a_y saturation at half slope of steer angle	41
7.2	Brushing process: on the right final postprocessed data, on the left raw data	42
7.3	Final raw data after postprocessing with filtering (brushing and normalisation to origin)	42
7.4	Final raw data with limited ramp slope and no postprocessing . . .	43
7.5	Vertical loads behavior: left picture Fz in Ramp1 for the different wheels, right picture $F_{z,FL}$ in different ramps	45
7.6	Set of raw data, plot 3D with $F_y(\alpha, F_z)$	46
7.7	Burckhardt resultant friction coefficient: left Matlab result for Hoosier tires, right typical cohesion coefficient characteristics (Book [15] Section Vehicle Modelling p.320)	48
7.8	Lateral wheel force F_{WS} for front left with Kiencke and Nielsen formulation	49
8.1	Curve Fitter Matlab with LMA	54
8.2	Lateral force characteristic, fitting with GA	55
8.3	Fitting with GA: change of dataset to limited ramp steer slope . . .	56
8.4	Fitting with GA: heuristic tyre model	58
8.5	Fitting with GA: Pacejka model with Fz, 3D plot	59
8.6	Comparison between the fitted tire models	60
8.7	Matlab functions for the tyre models	60
8.8	Simulated ramp steering, comparison of the fitted tire models in terms of lateral acceleration	61
8.9	A complete picture of the operation of the extended Kalman filter [19]	64
8.10	States behavior of the EKF with respect to the measurements in ramp steering simulation	67
8.11	Ramp steering simulations with the signals of a_y corrected by EKF and the logged data	67
8.12	Ramp steering simulations with the signals of a_y coming from: the logged data, the tire models and the simulations corrected by EKF	68
8.13	Ramp3 and Ramp8 simulations with the signals of a_y from logged data and the simulations corrected by EKF	68

9.1	Testing cycle in lateral dynamic for Hoosier 43075 16x7.5-10 LCO from TTC	71
9.2	Cornering test Lateral Force Fy for Hoosier 43075 16x7.5-10 LCO from TTC	71
9.3	Cornering test, lateral Force Fy comparison Hoosier 43075 16x7.5-10 LCO and Hoosier 43075 16x7.5-10 R20 from TTC	72
9.4	Comparison of the lateral Force Fy between TTC lab data, experimental track test data and Pacejka fitted model	74
9.5	Lateral Force between TTC lab data at Fz=444 N and Fz=667N, experimental track test data and Pacejka fitted model	74
10.1	Tables for averaged and maximum errors in the lateral acceleration between tire models and logged data	75

Chapter 1

Introduction

1.1 Formula Student Competition

Formula Student is an international engineering competition for university students that challenges teams to design, build and race a Formula-style racing car. Formula Student provides a platform for students to apply their theoretical knowledge in a real-world environment and to develop skills in teamwork, communication, leadership, innovation and entrepreneurship.

Formula Student aims to develop the next generation of engineers, innovators and leaders in the automotive and motorsport industries and to promote sustainability, safety and affordability in motorsport. The competition involves a series of static and dynamic events that test the performance, reliability and cost effectiveness of the cars. The events are:

Static events:

- **Engineering Design Event:** teams present their car design to a panel of judges who assess the design, innovation and feasibility of the car. The judges may ask questions to test the team's knowledge of the car's design, validation and engineering principles.
- **Cost and Manufacturing:** teams present a cost report detailing the cost of materials and manufacturing processes used in the design and production of the car.
- **Business Plan Presentation:** All teams present a business case for their car, detailing the marketing and sponsorship strategies, financial planning, and sustainability aspects of their project.

Dynamic events:

- **Acceleration:** A simple straight line acceleration over a 75 meter track, the fastest car wins. Traction and low drag are the key to winning this event.
- **Skidpad:** In this event the car must complete a figure of eight pattern, driving 2 laps of the right circle and 2 laps of the left circle. The second lap of each circle is timed and the average of these times plus any penalties is the total time of the run. This event tests the car's cornering grip and stability.
- **Autocross:** This event is like an F1 qualifying session. Drivers race around a technical track full of tight corners, chicanes and slaloms. The event tests the car's handling, agility and driver skill.
- **Endurance & Efficiency:** The endurance event evaluates the durability and reliability of the car by testing its performance over a long distance, the track has the same characteristics as the autocross and the total event is about 22 km long. At the end of the course, the total energy consumed is calculated, taking into account the amount of energy recovered as a negative contribution. This is how the efficiency ranking is determined.

To participate in Formula Student, each team must design and build a single-seat, open-wheel, formula-style race car that meets a set of technical regulations and safety standards. To take part in the dynamic events, the team must pass a series of technical inspections and tests, such as the electrical inspection, mechanical inspection, brake test and rain test. The future of Formula Student is a promising one, as the competition continues to evolve and adapt to the changing landscape of motorsport and mobility. The competition embraces new technologies such as autonomous driving, electric and hybrid powertrains, advanced materials and manufacturing methods. Overall, Formula Student is an exciting and rewarding programme that offers students a unique and valuable experience in the world of engineering and motorsport.

1.1.1 RWTH Ecurie Aix

The RWTH Ecurie Aix is a strong group of around 70 students from the RWTH Aachen University, they are well organised and with a large Alumni network. The already graduated students are always available to provide the proper support to the new members, with videocalls and reviews, in order to ensure the good transmission of knowledge through the following generations. This process is ensuring great results. The team has reached astonishing achievements in the last years, remarkable is the 1st place in the hardest competition, FSG Formula student Germany, in the 2023. Also in the last season the team has achieved successes, such as the 2nd overall place in Formula Student Netherlands. The aim of this project is to improve the performance of the car with a deeper knowledge of

tyre behaviour. The topic has been proposed by the "Performance" group in the "LapTime Simulation" department. The support of the team will be provided through the introduction to the software used to analyse the data collected from the car, the projects developed in the past years as the Simulink model "LapTime Simulator", material support for the track tests.

1.1.2 Tyre impact on Formula Student

The thesis represents a novelty in the Formula Student environment, especially because of the use of real data. The teams can afford to have an account with the Tire Testing Consortium (TTC), a tyre testing laboratory in Calspan, where several of the components have been tested. This is a good tool for evaluating tyre performance, but it has some limitations. Firstly, the tyres most commonly used by the Formula Student teams are the 10-inch Hoosier compound, and this type of tyre has not been tested in longitudinal dynamics by the TTC. This lack of data and knowledge is a significant limitation for the teams. In addition, the laboratory provides data that has not yet been compared with real data. The friction and grip levels obtained on the tyre testers are obviously not in line with the normal track conditions of the Formula Student Championship. The aim of this work is to overcome these problems, the real data will only be collected in lateral dynamics in order to have values that can be compared with the TTC. It is worth noting that the tyre is a crucial component in the design of a racing car. All of the team's efforts in powertrain and mechanical design need to be exploited as forces on the ground. The grip of the tyres can be a bottleneck if not properly designed. The choice of tyres is therefore an important aspect of the Ecurie Aix team's project. This season, the team has decided to test two different Hoosier compounds: Hoosier 43075 16x7.5-10 LCO and Hoosier 43075 16x7.5-10 R20. The only difference is the material and the hardness of the surface, the main dimensions have been confirmed by previous years' tests. A brief comparison using TTC data is given in one of the following paragraphs. More details on the tyre's behaviour can be found in the chapter chapter 3.

1.1.3 Equipment and Sensors

This section briefly describes the equipment used in the tests of the thesis. Only the sensors that are useful for the specific test will be discussed. The main sensor used by the team is the SBG Ellipse-N. This is a high performance Inertial Measurement Unit (IMU) designed for motion sensing applications such as racing cars, making it particularly suitable for Formula Student. This compact and lightweight sensor integrates a multi-band RTK (Real-Time Kinematic, a satellite navigation technique) GNSS (Global Navigation Satellite System) receiver, enabling

precise positioning to centimetre accuracy. The Ellipse-N offers high orientation performance with a roll and pitch accuracy of 0.05° RMS in real time conditions and a heading accuracy of up to 0.2° when using GNSS augmentation. These features are critical for capturing the dynamic behaviour of the vehicle with high accuracy. These characteristics are highly demanded by the driverless group: the Ecurie Aix team is competing with the same car in the human driver and autonomous categories. In terms of mechanical characteristics, the Ellipse-N is remarkably compact, with dimensions of 29.5 x 25.5 x 16 mm. It weighs only 17 grams, minimising its impact on the overall vehicle mass. The rugged design ensures reliable operation in harsh environments and can withstand shocks of up to 500g. The sensor communicates via the Controller Area Network (CAN) interface, a robust vehicle bus standard that allows microcontrollers and devices to communicate without a host computer. This feature facilitates easy integration with the vehicle's data acquisition systems and enables real-time data transmission, essential for telemetry analysis in Formula Student. The other sensor used is a steering angle sensor, the Euro-CMRK-A-111-1216-360-17-50. The steering angle measurement system uses the Euro-CMRK Hall-effect sensor, which offers a good balance between accuracy and compact design for racing applications. It is a non-contact rotary position sensor in an anodised aluminium housing, making it particularly suitable for the space-constrained Formula Student steering assembly. With an outer diameter of 21.5mm and a thickness of 6.6mm, the sensor is integrated into the steering column. The assumed range of the driver's steering angle in the vehicle is the interval (-120, 120) degrees. The sensor is capable of providing a full 360 degree measurement range with $\pm 0.5\%$ independent linearity, making it perfectly suited to its application.

Chapter 2

State of art

In this chapter a brief analysis of the state of art, relative to the methodologies used in scientific researches, is shown. In particular, the different possibilities of approach to determine the tire forces are reported.

2.1 Researches on sensors

The problem of measuring the tire ground contact forces arises when the dynamics of the pneumatic system is not completely clear. This mathematical problem is better described in the chapter chapter 4. To overcome the inaccuracies of the physical model of the tyre compound, a direct measurement is used. There are several possibilities. The sensors used in a laboratory test machine are based on the Wheel Force Transducer (WFT). This is a multiaxial precision measurement system, more precisely a 6-component measurement system, capable of measuring three forces and moments on a rotating wheel. It is widely used in laboratories and can be mounted directly on the wheel hub. One of the main manufacturers is Kistler, a company that develops specific sensors for the automotive sector. The description of this sensor on their website states: "Wheel force transducers are designed for use in the development and testing of complete chassis and chassis components of various vehicles such as passenger cars, SUVs, commercial vehicles, racing cars and industrial vehicles. During measurement, a wheel force transducer replaces a standard wheel and measures the forces and moments acting on the tire contact patch.[1]" There is no other component between the road and the vehicle hub other than the tire and the mechanical structure of the wheel force transducer, so this design allows a rather direct transmission of loads. Most scientific papers use this technology to validate wheel load estimates, an example of which is reported in the paper [2]. The main drawback of the WFT is its high cost. As a student team, the price asked for one of these sensors was beyond our budget. An effort was made

to get more information and get the lowest price. After several meetings, the best offer was around €6250, made by Bota Systems, a start-up company from the ETH Zurich. Other interesting sensors that can provide measurements related to wheel loads are "strain gauges". A strain gauge is a sensor whose measured electrical resistance varies with changes in strain, i.e. deformation or displacement of material. Strain gauges convert the applied force, pressure, torque, etc. into an electrical signal that can be measured. Force causes strain, which is then measured by the strain gauge through a change in electrical resistance. The strain measurement is then collected using data acquisition. These devices cannot be mounted directly on the wheel, but a good analysis can be made by positioning them on the suspension arms. Knowing the suspension geometry and the inertia of the wheel hub assembly, the forces measured on the suspension arms can be converted into tyre contact forces. This solution is an indirect measurement, but the position of the strain gauges is close enough to the wheel to overcome many inaccuracies. Very accurate results can be achieved, but there are several disadvantages. The first is cost; the strain gauges are very cheap, but the extensometer electronic control unit is expensive. Without this component, the electrical signal cannot be converted. Finally, this system requires long and hard work to calibrate the strain gauges. For these reasons, the solution of using strain gauges was discarded. For the sake of completeness, an interesting article on a new type of sensor is reported [3]. It concerns "intelligent tyres", a modern construction of a wheel in which an accelerometer is mounted inside the tyre, between the rim and the tread. This technology is not only able to measure the wheel loads through the accelerations, but it also gives important data about the length of the contact patch. This solution is capable of providing a complete understanding of the wheel characteristics and could also be more accurate than the wheel force transducers. The main drawback is the high complexity of the system to be implemented on the wheel assembly, especially when dealing with small tires such as those used in Formula Student cars.



Figure 2.1: WFT Megaone from Bota Systems



Figure 2.2: Strain gauge on a suspension arm

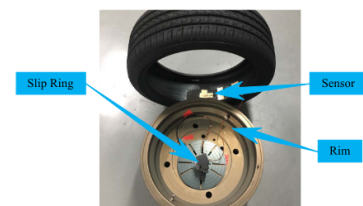


Figure 2.3: Intelligent tire, accelerometer in the wheel

In the following paragraph the last and adopted solution for this thesis is presented.

2.2 Estimation methodologies

Most of the scientific papers use different estimation techniques to evaluate the tyre ground forces. The starting point is the use of cheaper sensors such as GPS and IMU (Inertial Measurement Unit). In this way, the experimental data collected by the car are not close to the wheel, but are global parameters of the vehicle, such as lateral and longitudinal accelerations, vehicle speeds, yaw and roll angles. To obtain tyre force values, a vehicle model is required. There are basically two possibilities: build an accurate vehicle model with many degrees of freedom, or use a simpler vehicle model and correct it using control techniques. The accuracy of the values obtained increases as the mathematical model becomes more detailed, bringing them closer to real-world data. However, this level of complexity requires significant computational resources. On the other hand, the model can use the obtained values to perform a detailed analysis of the vehicle dynamics. Conversely, a simplified model reduces the computational load and still provides accurate values when compared to real data. However, such a model is limited in its ability to analyse vehicle behaviour as it is restricted to the specific conditions used during the identification process. Finally, the second approach is the most widely used and provides accurate results, usually validated by experimental measurements using one of the sensors described in the previous section. The control systems that can be used in this way are very different. An example of a complex control strategy is the cascade observer structure developed in the paper by Rafael A. Cordeiro [2]. He uses three different observers to estimate the vertical, longitudinal and lateral forces, and finally an unscented Kalman filter to correct the calculations by comparing them with the direct measurements. The use of a Kalman filter is the most widely used, as it represents an optimal control technique capable of managing conditions in a fast and reliable way. Another example is reported in 2.2.1, it concerns an interesting study focused only on the lateral dynamics made by the researcher J. Kim [4].

2.2.1 Control system technologies, focus on EKF

Most of the efforts in this field are made to collect reliable data for autonomous driving. This means that the control techniques should be able to calculate the tyre parameters online, quickly and reliably, in all the different road conditions. Most of the complexities arise when the objective is to develop a system that can be implemented in everyday passenger cars. Given this aim, it is not possible to rely on expensive sensors. The tyre parameter problem is intrinsically non-linear, which

suggests the use of an Extended Kalman Filter, EKF. J. Kim [4] has developed a 4 dof vehicle model and an Extended Kalman Filter based on a combination of IMU and GPS that measures lateral acceleration, longitudinal and lateral velocities, roll and yaw angle derivatives.

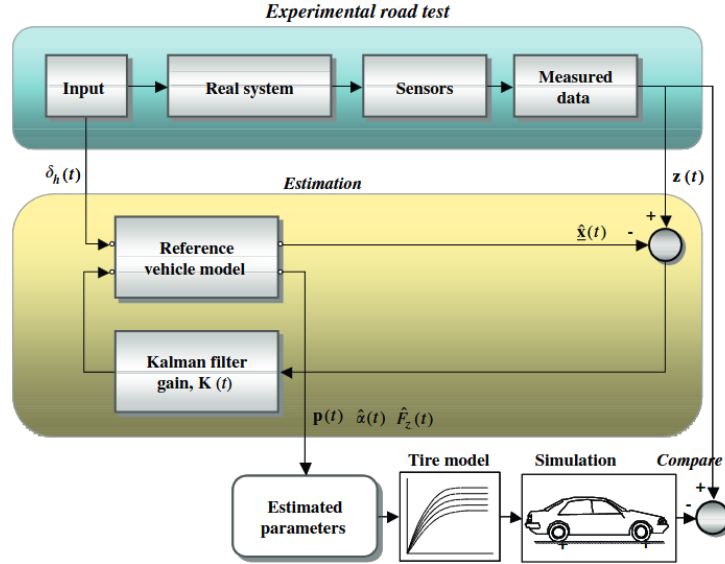


Figure 2.4: Graphical scheme of the procedure adopted to estimate tire model parameters

The figure 2.4 shows the loop of the strategy. The measured data is used as a reference for the states calculated in the vehicle model. The difference between these two quantities represents an estimation error, which is fed into the Kalman filter to correct the inputs to the vehicle model. Through this closed-loop feedback, after several iterations, the filter is tuned so that the outputs of the 3 dof model match the actual measurements. The lateral forces at tire ground contact are part of these outputs. As a consequence, these values can now be considered reliable for use in a fitting procedure that extrapolates the tyre parameters. The tire model used is the Pacejka Magic formula, for a more detailed description see chapter 4. The study [4] avoids complex and expensive sensors, moreover the chosen approach, based on a simple model with a correction technique, make it a good reference for the work of the thesis. Another similarity is the focus on lateral dynamics. The Hoosier 43075 16x7.5-10 LCO, the tire chosen by Ecurie Aix, has been analysed by the tire testing consortium only in terms of lateral dynamics. This meant that the thesis aimed to model lateral forces using real data. At the end of the work, it will be possible to compare the laboratory results with the estimates obtained from the simulations. The thesis is also a valuable reference for the manoeuvres

carried out, more details in the chapter 6. The focus is on the Extended Kalman Filter, which, as is well known, has a high reliability for observing states and parameters simultaneously. These characteristics make the EKF the necessary tool to avoid expensive instruments. The identification technique used in the paper, the continuous extended nonlinear Kalman filter, requires both the model and the measurements to be available as continuous functions of time. To achieve this, the measurements must be sampled at a high enough frequency so that they can be transformed into continuous data during the execution of the algorithm by linear interpolation. The states are the quantities that the Kalman filter aims to predict, but the measurements are the references that come from the real world. An interesting feature of the EKF is the operation that maintains its dynamics. It is based on two phases: Time update or prediction phase, measurement update or correction phase. The first is the calculation of the states, through the equations that hold the model. It represents a prediction, since these results are in the future, following the time step. The correction phase is performed through the Kalman gain matrix and the covariance matrix P. In this way, the Kalman filter has a probabilistic aspect, it introduces random variables as noises both on the process and on the measurements with normal probability distribution. A detailed description of the EKF design can be found in the reference [5]. In the paper described above, the state vector has 7 components:

$$x(t) = [v_x(t), v_y(t), r(t), \phi(t), F_{yf}(t), F_{yr}(t), p(t)]$$

With $\phi(t)$ yaw angle and $r(t)$ derivative of the roll angle. The last component, $p(t)$, is the vector of the parameters to be defined:

$$p(t) = [B_f, D_f, E_f, B_r, D_r, E_r, \sigma_f, \sigma_r, F_{xd}, \dot{F}_{xd}]$$

It contains the Pacejka parameters for the front and rear axle, the relaxation lengths and the longitudinal drag force (that includes aerodynamics drag force and rolling resistance) with its derivative. Instead, the measurement vector is

$$z(t) = [v_x(t), v_y(t), r(t), p(t), a_y(t)]$$

where $p(t)$ is the derivative of the yaw angle. In this way the state vector has about 17 components and the measurement vector has 5 components. This applies to a large number of differential equations calculated for each time step, and the updating of the Jacobians (derivative of the system equations with respect to the vector of parameters p) requires a large computational effort. The number of simultaneous equations is 170, at each time step 374 numerical derivatives have to be computed for the Jacobians. As the EKF uses statistical information, it requires several identification runs to obtain more reliable results. The values obtained in one iteration can be used as initial values for the next integration cycle. This large computational effort is not reproduced in the work of the thesis, but the general workflow described has been considered as a good reference.

Chapter 3

Tire Behavior

The tire is a fundamental component of a racing car, as most of the performance depends on how well its behaviour is understood. In a Formula Student team, great results, in terms of vehicle dynamics, can be achieved by analysing the grip of the wheels. The tire becomes a crucial element from which experimental studies can be carried out. From a mathematical point of view, it is still an area that leaves place for deep research and continuous development. In this thesis, a brief introduction to the subject is given, considering the notes of the book "*Milliken & Milliken Race car vehicle dynamics*"[6].

The interaction between the tire and the road provides the traction, braking and cornering forces for manoeuvring. Tyres support the weight and any vertical force, and it is to its needs that the aerodynamics are developed (in terms of downforce as a normal force for the pneumatics). These forces affect the vehicle in many different ways. For example, steering torques are generated by the tires and affect the driver's feeling; the steering system is designed from the tire torques. Temperature, pressure and speed all affect the tires. In this thesis, they are studied only in the generation of lateral forces, which are of primary interest in cornering. Some basic concepts are now reported, just as introduction to the topic. The area of the tire in contact with the ground is called the footprint or contact patch. The rubber elements can stick to the road or slide over it. There is not yet a complete understanding of how the rubber elements stick and slide. Sticking is a mechanical process that depends mainly on the hysteresis of the material when it is subjected to compression and relaxation during the rotation of the wheel. So a large part of the grip is determined by a mechanical process. The molecular adhesion is a lesser part of the grip, with the chemical and/or physical interaction between the atoms of the tread and the road surface.

A lateral force comes from the centre of the contact patch and is perpendicular to the direction in which the wheel is heading, if there is no camber angle. The latter is the angle of inclination of the wheel as seen from the front of the car.

To analyse the lateral behaviour of the tire, it is worth considering a model in which a constant vertical force and a lateral force are applied. During the rotation, imagine a contact point in the footprint: when it enters, it is subjected to a lateral displacement, since the tire behaves like a spring, it reaches a maximum deflection then, when it approaches the trailing edge, the spring behaviour brings it back to the undeformed state. This displacement is due to the frictional force between the contact point and the road. When the static friction limit is exceeded a lateral force is exploited and the tire begins to slip. In this way the model is deflected sideways and rolled, so the tire moves in one direction at an angle called the 'side slip angle' (see in the book [6] section Tire Behavior - Section 2.1 pp.18-20). A higher lateral force means a higher slip angle, looking at the contact patch this means that the onset of slippage is moved forward to the front of the footprint.

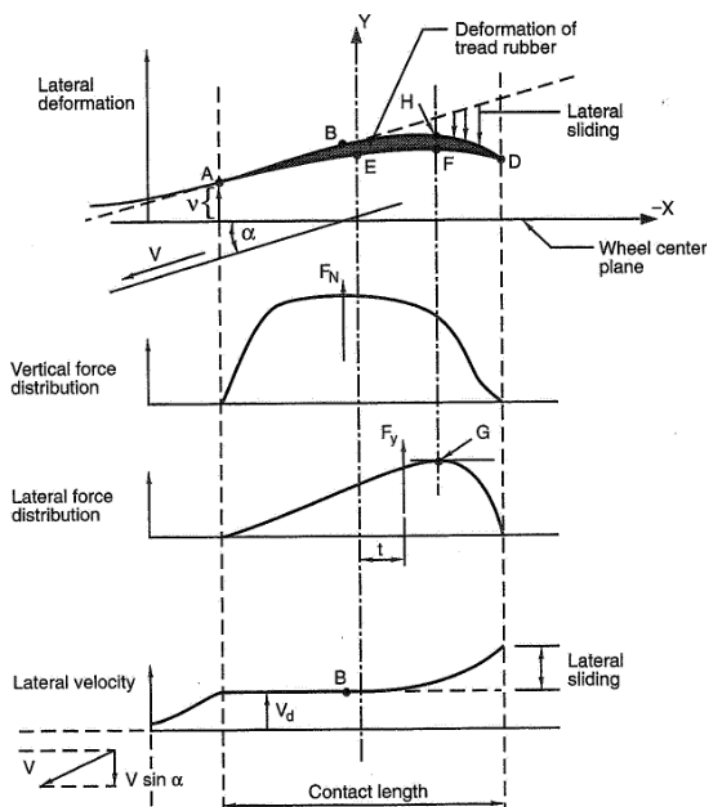


Figure 3.1: Deformation of the footprint and distribution of forces over the contact patch

The upper part of the figure 3.1 shows the distortion of the footprint, from which the "pneumatic trail" can be defined. It is the distance between the centroid of the footprint and the actual point of application of the lateral force. The "tire

aligning torque" is the product of the "pneumatic trail" and the lateral force. It is a moment that tends to realign the tire in the direction opposite to the lateral slip angle. In the third graph, the letter *t* indicates exactly the "pneumatic trail".

Laboratory and on-road test machines are used to measure lateral forces. Both are described in the following chapters. An example of the lateral force characteristic is reported in [7].

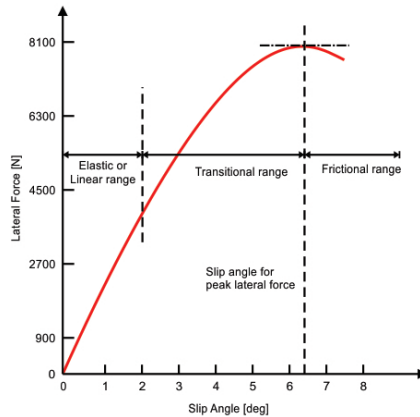


Figure 3.2: Side lateral force vs slip angle

The figure 3.2 shows the cornering force versus slip angle for a racing tyre. There are three regions: the linear region, which is described by the cornering stiffness, i.e. the slope of the line; the transitional region, where the maximum force is reached at its extreme limit; finally the frictional region, where the slip completely affects the footprint, causing a reduction of the grip. In general, the peak of lateral force is reached between 3° and 7° . On wet surfaces the peak will be lower and the drop will be faster. The influence of various factors on lateral force will now be explained.

3.1 Normal Force F_z : load sensitivity

The normal force (F_z) is the amount of load at which a tyre is imposed, in a race car different factors determine the value of it especially in dynamic condition. These will be better explained in the chapter 7. In general as the load increases the peak of lateral force is shifted towards higher slip angle and at higher values. Also the cornering stiffness increases 3.3.

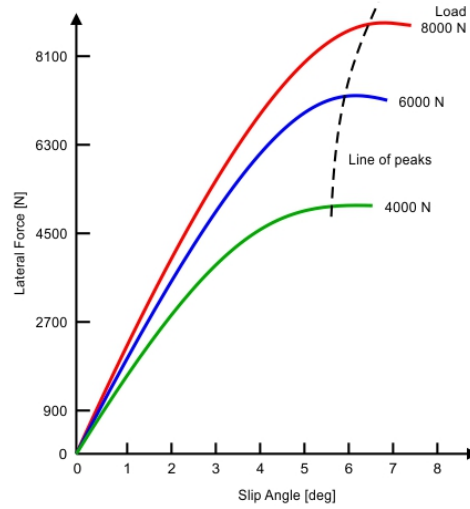


Figure 3.3: Effect of F_z on F_y vs slip angle [7]

In the following an important rule is played by the friction coefficient, defined as:

$$\mu = \frac{F_y}{F_z} \quad (3.1)$$

It is a dimensionless measure of the amount of lateral force with respect to the load. It can also be seen as frictional force between two bodies over normal force between them. Due to the road characteristics the fact that different values of μ are obtained, between laboratory and track, have to be taken into account. The tire load sensitivity is the phenomenon for which the peak of lateral friction coefficient falls off as load increases. This effect in a race car is affecting the balance since the tyres are working near the limit.

3.2 Inclination angle or Camber angle γ

Camber angle is defined as the angle between the vertical and the titled wheel plane. In tyre testers following the SAE Tire Axis System, camber is positive when the wheel is tilted outwards at the top relative to the vehicle. The nomenclature inclination angle is used in relation to the tilt of the wheel. A wheel in the tester has a positive inclination angle if it is seen tilted to the right behind the rolling tyre. In racing, the inclination of a wheel is called camber. A cambered tyre produces a lateral force in the direction of the tilt, when this occurs at zero slip angle it is called camber thrust. For wide street radial tyres, the camber force has a small

effect on the slip angle force, and the peak of camber thrust is at 5° and then decreases rapidly. (book [6] Tire Behavior - Section 2.5 pp.46-47) In racing tyres, the maximum force due to camber occurs at smaller angles. Different case for motorcycles, where this effect has a high impact on performance.

The camber also has an effect on the alignment torque, causing a distortion of the print which results in an increase in the slip angle. To prevent the alignment torque from being cancelled out by the combination of slip and camber angle, it may be necessary to increase the mechanical trail. The lateral force F_y versus slip angle α is translated up and down by camber. This is only true in the linear range where camber thrust and lateral force are additive, but the roll-off is reached when the linear range is exceeded and the camber effect is reduced. The peak of the cornering curve is obtained with negative camber values, i.e. when the tyre is tilted inwards into the corner.

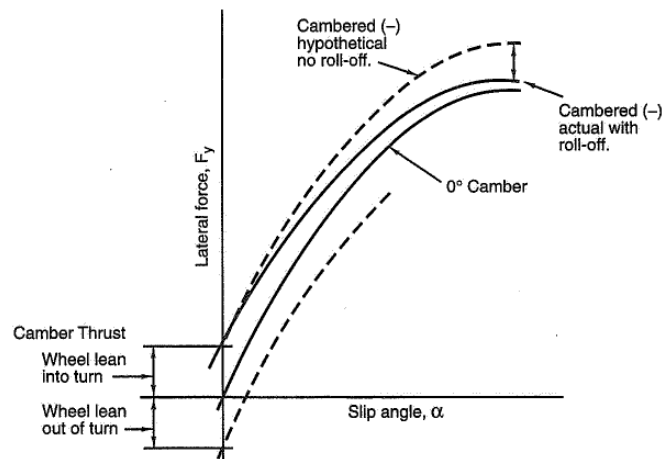


Figure 3.4: Camber effect on lateral force and roll-off [6]

Maximum lateral force is obtained at higher camber angles when the normal load on the tyre increases. In a racing car it is used to tilt the wheels on the same axle cambered inwards.

3.3 Pressure

One of the simplest changes that can be done to the set-up of a race car is about the tire pressure. It affects performance in a number of ways. The tire manufacturer set the range of permissible pressures, this means lower and higher values are here said with reference to a range of pressures. Cornering stiffness is increased as the pressure is raised because the carcass becomes stiffer. This means that in the linear

range, i.e. for small side slip angles, increasing pressure results in an increase in lateral force. In terms of friction, lower tire pressure promotes contact between the rubber tread and the road, resulting in a higher effective coefficient of friction. Another effect is an increase in contact patch. The disadvantage of lower pressure is an increase in steering effort during lateral acceleration due to lower cornering stiffness and an increase in alignment torque. The consequence of too low a pressure is the formation of high pressure areas at the sides of the tire, mainly due to the stiffness of the sidewalls. To avoid this, the pressure is generally set so that the centre and edges of the tread carry a proportional load. Rolling resistance, or the energy lost in deforming the tire, is reduced at higher pressures thanks to the smaller footprint. Induced drag, the energy lost when cornering, is reduced with higher pressure. This is due to the lower slip angle required to develop lateral force. Finally, tire pressure is a compromise between tread performance and grip, the former achievable at high pressure and the latter at low pressure. Only through experimental testing can the best value be found for each specific car. (book [6] Tire Behavior - Section 2.6 pp.54-55)

3.4 Temperature

The effects of temperature are related to wear and performance. The higher the temperature, the shorter the life of the tire. The main reason for this is the melting between the tread and the road. In the work of this thesis, this effect is less relevant in terms of the consequences on the performance of the pneumatic. It is important to distinguish between the possible measurements that can be taken. The internal temperature is an average between the rim and the tread, it is complex to measure with cheap sensors. In this work, the temperatures collected are relative to the surface of the tyre. It is possible to understand different characteristics just by taking temperatures at different points of the wheel tread. For example, a high value of camber angle leads to a hotter inner part of the tread. Cornering stiffness is affected by a change in temperature because it changes the modulus of elasticity of the tyre. The effect of temperature is closely related to pressure, with lower initial pressure resulting in a stiffer tyre and therefore higher temperatures. If the tyres are too cold, they will be slippery, but if they are too hot, they will melt on the contrary. Maximum grip is achieved at an optimum temperature, generally the best way to obtain data on this is to test and rely on the data provided by the suppliers.

Chapter 4

Pacejka Magic Formula

This chapter presents the most commonly used tire model. The focus of the work is on lateral dynamics, more specifically the lateral force model during cornering. For this reason, all the presented notes deal only with lateral dynamics. More details can be found in the book by Pacejka [8]. It is worth noting Pacejka's definition of pure slip, i.e. when either longitudinal or lateral slip occurs in isolation. It is possible to see that the curves exhibiting a shape like the figure 3.2 can be represented by a mathematical formula called the " Magic Formula ". This is a semi-empirical tire model for calculating steady-state tire forces. The formula is the result of a collaboration between TU Delft University and Volvo in 1996. The original formula is given below, it is valid for fixed values of vertical load F_z and camber angle γ .

$$F_y(\alpha) = D \cdot \sin[C \cdot \arctan(B \cdot \alpha - E(B \cdot \alpha - \arctan(B \cdot \alpha)))] \quad (4.1)$$

The input variable, in that case, is the side slip angle α , but in some other formulations it is also possible to see the lateral slip as $k = \tan(\alpha)$. The parameters to be determined in this thesis are here presented:

- B: stiffness factor;
- C: shape factor;
- D: peak value;
- E: curvature factor.

Normally, this mathematical equation produces a function that crosses the origin and, after a maximum peak, tends to an asymptote. The shape is anti-symmetric with respect to the origin. The cornering stiffness or slope at the origin is given by the product BCD. Among these three terms, B is called the stiffness factor, since

the others are chosen to control other characteristics. D is responsible for the peak and is strictly related to the friction coefficient μ and the vertical force F_z .

The shape factor C defines the limits of the sine wave in terms of its range.

Finally, the horizontal position and the curvature at the peak are controlled by the E term.

In the pictures 4.1 it is possible to visualise the effect of varying the individual parameters.

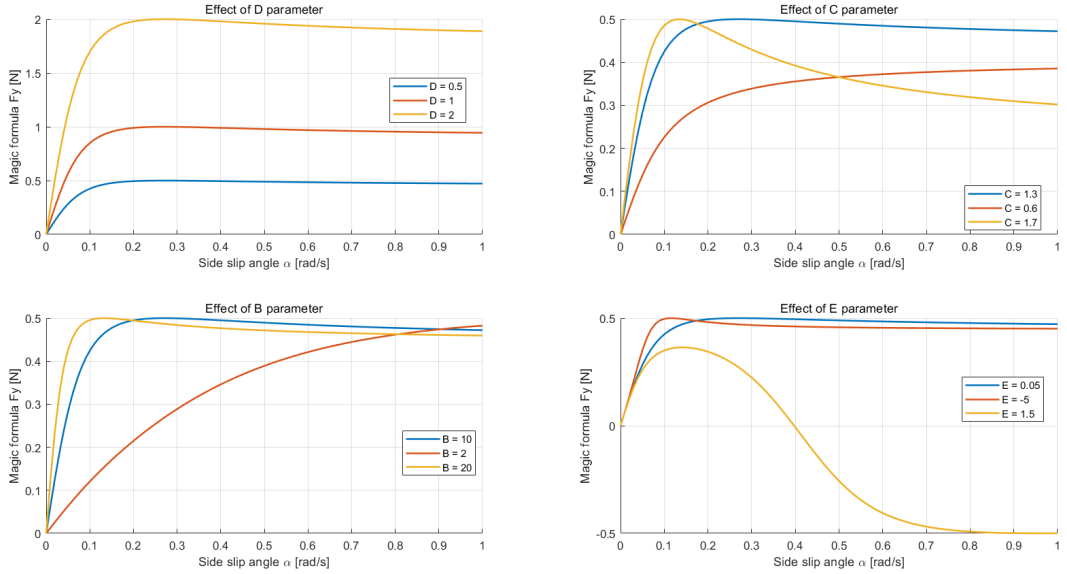


Figure 4.1: Sensitivity analysis of the Pacejka parameters B,C,D,E

In some extreme cases, it is needed to add a parameter H to have an increased sharpness of the curves:

$$F_y(\alpha) = D \cdot \sin[C \cdot \arctan(B \cdot \alpha - E(B \cdot \alpha - \arctan(B \cdot \alpha) + H \cdot \arctan^7(B \cdot \alpha)))] \quad (4.2)$$

All the factors described are dependent on the physical variables described in the chapter 3. The Pacejka formulation describes the factors focusing on the dependence on normal load and camber angle. For the determination of B,C,D,E a regression technique has to be used, different methods are described in the following chapter 7. A very complex set of equations is described in Pacejka's book [8], but the regression technique used in the thesis is based on direct identification of parameters B,C,D,E. The full set of equations presented in Pacejka's complete tire model requires the knowledge of tire parameters not available from the team equipment. The dependence of the mathematical parameters on variables such as normal load, camber angle, internal pressure and temperature is difficult to

take into account because the available sensors do not measure these variables directly. Moreover, most studies carried out on real track data do not rely on the dimensionless parameters and scaling factors introduced in the full set of equations, but only on the main coefficients D, C, B and E. In the following 6 the way in which these effects are considered in the track tests is described. The complete Pacejka model equations have been reported in the following for completeness.

$$\alpha_y = \alpha^* + S_{Hy}$$

$$C_y = p_{Cy1} \cdot \lambda_{Cy}$$

$$D_y = \mu_y \cdot F_z \cdot \zeta_2$$

$$\mu_y = (p_{Dy1} + p_{Dy2}df_z)(1 + p_{py3}dp_i + p_{py4}dp_i^2)(1 - p_{Dy3}\gamma^{*2})\lambda_{\mu_y}^*$$

$$E_y = (p_{Ey1} + p_{Ey2}df_z)(1 + p_{Ey5}\gamma^{*2} - (p_{Ey3} + p_{Ey4}\gamma^*)\text{sgn}(\alpha_y))\lambda_{Ey}$$

$$K_{y\alpha} = p_{Ky1}F'_{z0}(1 + p_{py1}dp_i)(1 - p_{Ky3}|\gamma^*|) \cdot \sin\left(p_{Ky4} \arctan\left(\frac{F_z/F'_{z0}}{(p_{Ky2} + p_{Ky5}\gamma^{*2})(1 + p_{py2}dp_i)}\right)\right) \zeta_3 \lambda_{Ky\alpha}$$

$$B_y = \frac{K_{y\alpha}}{(C_y D_y + \varepsilon_y)}$$

$$S_{Hy} = (p_{Hy1} + p_{Hy2}df_z)\lambda_{Hy} + \frac{K_{yy0}\gamma^* - S_{Vy\gamma}\zeta_0 + \zeta_4 - 1}{K_{y\alpha} + \varepsilon_K}$$

$$S_{Vy\gamma} = F_z \cdot (p_{Vy3} + p_{Vy4}df_z)\gamma^* \cdot \lambda_{Ky\gamma}\lambda'_{\mu_y}\zeta_2$$

$$S_{Vy} = F_z \cdot (p_{Vy1} + p_{Vy2}df_z)\lambda'_{\mu_y}\zeta_2 + S_{Vy\gamma}$$

$$K_{yy0} = (p_{Ky6} + p_{Ky7}df_z)(1 + p_{py5}dp_i) \cdot \lambda_{Ky\gamma}$$

These equations contain non-dimensional parameters, p factors, and scaling factors λ . They are used to investigate, without implementing a new tire data set, the change of friction coefficient, cornering stiffness, camber stiffness. A better understanding is left to the reader through the source [8].

Chapter 5

Laptime Simulator

This chapter describes the main tool used in this thesis. The Laptime Simulator division in Ecurie Aix is composed by 15 students, that deals with the development of the Simulator. It is a tool on Matlab Simulink able to reproduce the behaviour of the car. At first sight, the model is very complex as it is entirely developed by the team in all over the years. This simulator is highly requested in the most important competitions of Formula Student. In the design of the car it is a fundamental tool to define the targets for the improvements of all the other groups. For instance, at the beginning of the season, LapTime provides the forces on the wheels. These are considered input for a multi body model on Adams to collect the loads at which the suspension system, for instance the rods of the wishbone assembly, is subjected. All the aspects that influences the performance of the vehicle are in the Laptime modelled. For instance, the battery and cooling have their own model with specific calculations, and the entire control system is developed in detail. This allows important design decisions to be made. For example, the effect on performance of increasing the battery capacity in relation to the increase in weight can be understood. The effect on the differential mass distribution can also be simulated. The different control strategies can be implemented and from the simulations the effect on performance can be analysed. For the sake of simplicity, only the general aspects of the tool are reported in this thesis. All blocks relevant to the work are described. After a brief introduction, the modifications to the Simulink model required for the thesis are described.

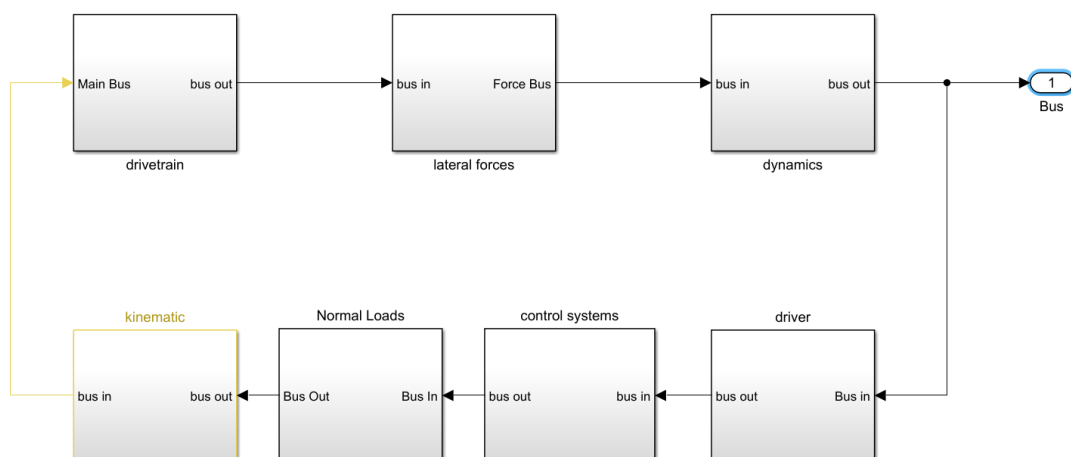


Figure 5.1: Laptime simulator loop

The figure 5.1 shows how the LapSim ¹ is structured. It takes as input the characteristics of the car, in terms of geometry and mass distribution, and the layout of the track. The track is provided as a Matlab struct, it is seen as a series of points representing the path. From these inputs a target velocity map is developed. During the events, the efficiency in terms of energy consumption is evaluated. In order to optimise it, LapTime is used to give the driver the lifting points. After a track walk, the path is computed. Thanks to the simulations, the efficiency of the different points of lifting is optimized. The locations of the lifting points are then shown to the driver on the steering wheel display. The GPS is the sensor that provides the updated position of the car with sufficient accuracy during the race. It is visible the loop that characterize the simulator. The Bus vector, marked in blue in the figure 5.1, contains all the variables calculated in each subsystem at each moment.

The "driver" subsystem contains the predictive model of the driver. In this block the basic command inputs are evaluated. For the lateral view, the steering angle is calculated taking into account a tunable parameter called lateral accuracy. In this sense, it imposes limits on the lateral acceleration, considering the distance from the theoretical path as an error. The model is based on a LookAhead approach, that means the steering angle is computed considering not only the immediate following point of the track, but weighting properly the 7 successive points. In terms of longitudinal dynamics, two constants are defined. They mainly represent the hardness of the accelerator and brake pedals. The corresponding pedal command is elaborated in terms of the target longitudinal speed and acceleration.

¹Abbreviation for Laptime Simulator

The next subsystem is the "control systems", where a version of the real control systems is implemented. Not all the calculations affect the LapSim, but the throttle and the torque to be applied to the electric motors are computed here. The command to the gas pedal is here limited based on the slip control, yaw rate controller and torque distribution. These blocks reproduce the real torque vectoring of the car, and their outputs are the torques applied to the wheels. The signals coming from the sensors in the real car are reproduced in this block. The maximum torque is evaluated using look-up tables that reproduce the engine maps, the input being the engine speeds.

The next subsystem works out the "Normal Loads". The static F_z , aerodynamic F_z , longitudinal and lateral load transfer components are computed. It is worth to notice that the aerodynamic normal loads, are elaborated through 4D LUT. The inputs are side slip, roll, pitch and steering angles, the outputs are lift and drag coefficients C_l , C_w . The choice of these coefficients depends on the longitudinal speed: 6 different LUTs can be selected, they are defined for $v_x = [11, 15, 18, 22, 25, 30]$ m/s. The data in the table have been extracted from the CFD analysis carried out by the Aerodynamics Group (updated periodically).

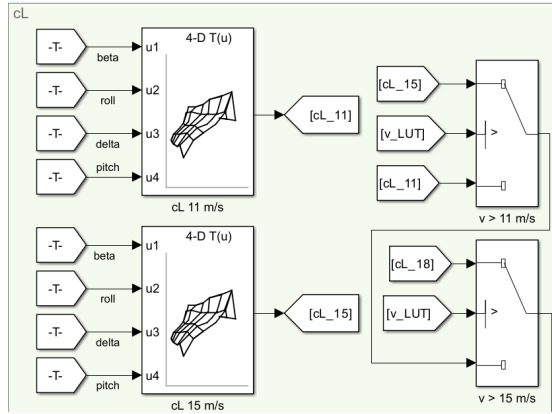


Figure 5.2: Example of aerodynamic 4D LUT for C_l evaluation

Moreover, the general loop in the LapSim is visible in that block, through the dependency of the lateral and longitudinal load transfer, to the accelerations a_y and a_x . In that computation the effect of the roll and pitch motion are taken into account, considering the torsional stiffness of the chassis, the sprung and unsprung masses contributions and the roll center location. The formulas are here reported.

$$USWT = \frac{m_{us}h_{us}}{l}a_y, \quad SGWT = \frac{m_s h_{pc}}{l}a_y, \quad SEWT = \frac{m_s(h_s - h_{pc})}{l}a_y \quad (5.1)$$

With h_{us} height of the barycenter of the nonsuspended mass, h_{pc} height of the

roll center and h_s barycenter suspended mass height. Then similar formulas for the longitudinal contribution, with a_x instead of a_y .

The additional pitch moment, APM, is also computed. With MR_f and MR_r motion ratios of front and rear, $c_{s,f}$ and $c_{s,r}$ elastic suspensions constants front and rear, $MR_{heave,f}$ and $MR_{heave,r}$ motion ratios for the heave, $c_{heave,f}$ and $c_{heave,r}$ elastic heave constants.

$$APM = 2l_{pc,f}^2 \left(\frac{c_{s,f}}{MR_f^2} + \frac{0.5c_{heave,f}}{MR_{heave,f}^2} \right) + 2(l - l_{pc,f})^2 \left(\frac{c_{s,r}}{MR_r^2} + \frac{0.5c_{heave,r}}{MR_{heave,r}^2} \right) \quad (5.2)$$

Also the dynamic radii are computed, they are based on the wheel normal loads that in input to a LUT are providing a difference with respect to the original dynamic radius. The LUT has five columns, one for a specific different value of tire pressure.

In the "kinematic" subsystem the camber, or inclination angle is analyzed. The final value is provided by the static value plus the contributions of steering rack travel and wheel travels. Both are evaluated through LUTs.

The next subsystem is the "drivetrain" in which there are the Battery Model, the Cooling analysis and the estimation of the front and rear longitudinal forces F_x . A Magic Formula 5.2 version is used for that target. Other blocks are here present for the slip ratios, torques and rotational wheel speeds estimations. Also the analysis of the brake moment is here conducted, starting from the driver brake signal. After all the longitudinal force is converted from the reference system of the wheel to the car RS, the presence of a toe angle is here considered.

The "lateral forces" subsystem presents lot of similarities with the previous one. The tire model, through the .tir file, is providing the values of F_y . These are rotated to the car reference system, and finally added to a vector containing the three x,y,z contributions of the wheel forces distinguished between front left, front right, rear left, rear right.

The last subsystem is the "dynamics". In that part the accelerations are elaborated through the balance equations starting from the wheel forces and moments. The longitudinal and lateral accelerations are coming from the Newton equations, in particular for the longitudinal equilibrium the rolling resistances and the aero drag force are considered. The global reference accelerations are then computed through the yaw rate $\dot{\psi}$. This last variable is coming out from the integration of the yaw acceleration. To compute it, a moment equilibrium is elaborated. The equations reported show what has been now described.

$$m \frac{dv_x}{dt} = F_{x,fl} + F_{x,fr} + F_{x,rl} + F_{x,rr} - \frac{M_{y,fl}}{r_{dyn,fl}} - \frac{M_{y,fr}}{r_{dyn,fr}} - \frac{M_{y,rl}}{r_{dyn,rl}} - \frac{M_{y,rr}}{r_{dyn,rr}} \quad (5.3)$$

$$m \frac{dv_y}{dt} = F_{y,fl} + F_{y,fr} + F_{y,rl} + F_{y,rr} \quad (5.4)$$

$$I_{zz} \frac{d\dot{\psi}}{dt} = aF_{y,fl} - \left(\frac{t}{2} + y_{\text{off}}\right) F_{x,fl} + aF_{y,fr} - \left(\frac{t}{2} + y_{\text{off}}\right) F_{x,fr} - bF_{y,rl} + \left(\frac{t}{2} + y_{\text{off}}\right) F_{x,rl} - bF_{y,rr} - \left(\frac{t}{2} - y_{\text{off}}\right) F_{x,rr} \quad (5.5)$$

Through integrations the yaw angle, the velocities v_x and v_y , then the positions are computed. As before, the rotation to the car reference system of a_x , a_y , v_x , v_y and ψ is performed. In this section also the side slip angles are estimated. In order to have all the variables at each time step, a delay block is needed. In that way it is possible to store for the previous time step the values of all the quantities necessary for the calculations in the other subsystems. All the quantities are finally assigned to the Bus to follow the loop.

In the following an example of a simulation output is shown. After the upload of the car characteristics and the track layout, without any additional script, the Simulink model is executed. A figure is opening during the simulation, where it is possible to follow the car motion through the track.

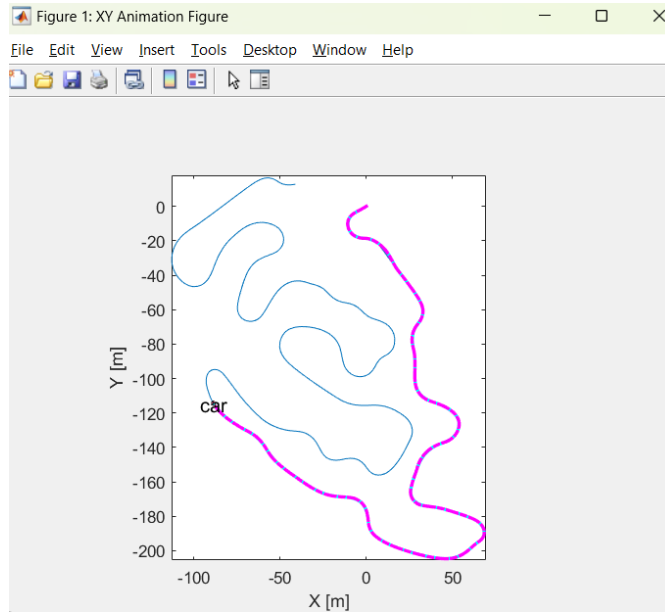


Figure 5.3: Figure output of LapSim simulation. Car data from eax02 on Autocross of FSG 2023

When the simulation ends, it is possible to see how the trajectory done by the car is following the path and tune it with the driver model parameters described at

the beginning of this chapter.

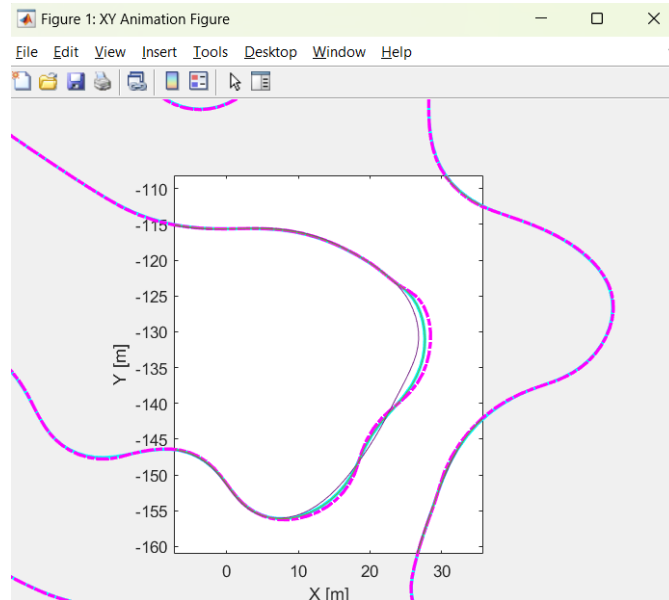


Figure 5.4: Trajectory analysis of the LapSim simulation. Car data from eax02 on Autocross of FSG 2023

In the picture 5.4 is it possible to see how the look ahead approach is working. The final trajectory doesn't match exactly the track path, in order to optimize the speeds in a corner entry and/or exit.

5.1 Logged data as input

LapTime, described up to now, is not able to receive as input the data coming from the sensors of the car. This is the first obstacle to be overcome, practically it means to convert a Simulation tool to a vehicle characteristics estimation tool. The sensors that provides the input data have been described in the section 1.1.3, basically the driver commands need to be preprocessed to run the new model. An overview of the new version is given in the picture 5.5.

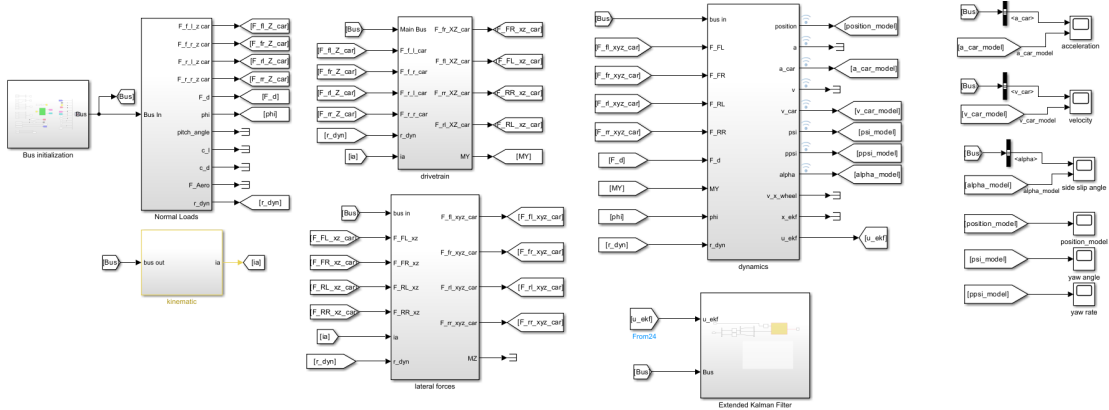


Figure 5.5: Overview of Thesis simulink model

It is possible to appreciate that the loop is no more present. Since the model needs to evaluate the lateral dynamics of the car by following the data coming from the sensors as input, the different subsystems are linked, but not in a circular way. The logged data is processed in the form of time-series signals. A deeper understanding of the process behind the export of the IMU and steering wheel sensor signals to Matlab is provided in the section 6.2. In order to run the model, a Matlab script must first be executed. In these simple lines, the time interval for the simulation is selected from the "Logdaten" structure, which contains all the experimental signals. The input driver commands are created as time series vectors, and additional useful reference signals are imported into the workspace. In this section the steering angle calibration error is performed, further description is given in the following 6. The logged signals used are

- Driver commands: braking "Log_PB_Brakeforce", steering "Log_SteeringAngle" and trottle "Log_PB_Torque";
- Vehicle global dynamics: longitudinal and lateral accelerations and velocities, yaw angle and yaw rate. All these are coming from the IMU, they are used as reference to check the results of the simulations. Only the accelerations are used as input for the vertical force load transfer;
- Wheel slip: longitudinal slip ratios and side slip ratios α for each wheels. Basically, these signals are used in the wheel force computation;

Some other variables are loaded, for instance the car characteristics and the tire parameters, and finally the simulation is started.

The "Bus Initialization" subsystem loads the logged signals and provides the conversion of them into the scales of the LapTime calculations. The driver's steering angle is first divided by the rack ratio to be expressed in the wheel reference system,

then by the Ackermann geometry to obtain the steering angle of the left and right wheels.

The normal loads computation is exactly the same as in LapSim with the only change of having the logged accelerations as input. Same considerations hold for the "kinematics" and the "drivetrain" subsystems, the latter uses the slip ratios as input from experimental data.

More complex modifications have been done for the "lateral forces" and "dynamics" subsystems. The lateral forces require the addition of Matlab functions to compute them through the parameters extracted experimentally, described in the chapter 7. The "dynamics" subsystem will be explained in details in the next section, it represents the core of the vehicle modelling.

Finally, a completely new subsystem is implemented with the Extended Kalman Filter, this step is described and used at the end of the thesis.

5.2 Vehicle model

In this section the model of the vehicle used in the Simulink project is described from a physical point of view.

A 3 degrees of freedom model is implemented, it is a rigid two-axle vehicle body model to calculate longitudinal, lateral, and yaw motion. It accounts for body mass, aerodynamic drag, and weight distribution between the axles due to accelerations and steering. The effect of the roll motion is considered in the load transfer, as already explained. The vertical motion is not considered in the model, but the pitch angle is used to determine the lift and drag coefficients of the aerodynamic forces. To determine the vehicle motion, the model implements these equations.

$$\begin{cases} m(\dot{u} - \dot{\psi}v) = \sum F_x \\ m(\dot{v} + \dot{\psi}u) = \sum F_y \\ J_z\ddot{\psi} = \sum M_z \end{cases} \quad (5.6)$$

With u and v longitudinal and lateral velocities in the car reference system. The resultant longitudinal force $\sum F_x$ takes into account the wheel loads, the rolling resistance and the aero drag. The resultant lateral force $\sum F_y$ is sum of the lateral forces coming from the tires. The moment around the vertical axle $\sum M_z$ is following the equation previously reported 5.5. The accelerations are equal to:

$$a_x = \dot{u} - \dot{\psi}v \quad (5.7)$$

$$a_y = \dot{v} + \dot{\psi}u \quad (5.8)$$

It is worth to notice that the yaw angle estimation is crucial to have good values of the velocities. In the following the simulink blocks are reported, to see the way in

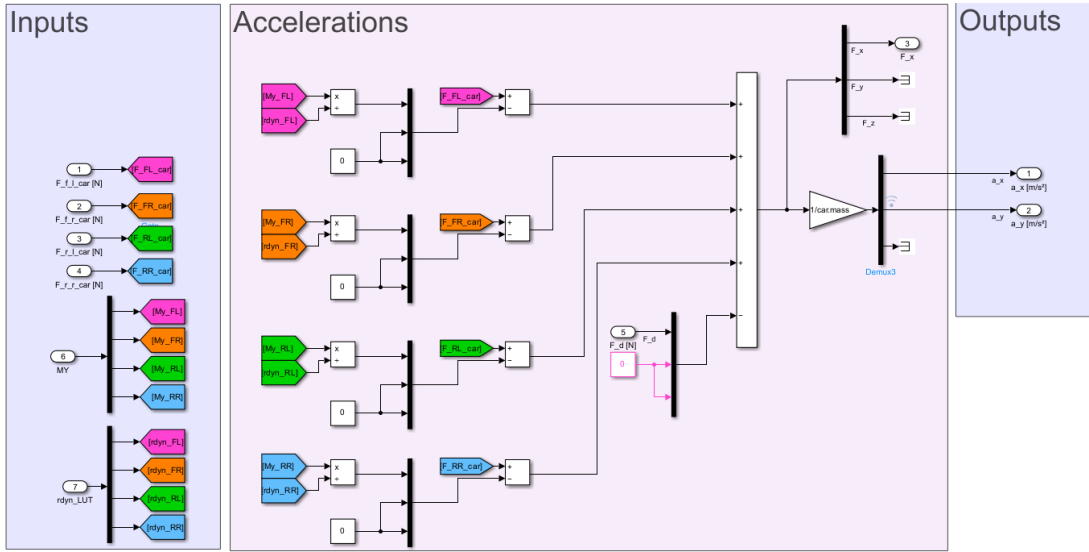


Figure 5.6: a_x and a_y equations in Simulink

which the equations of motion are implemented. The vectors of the wheel forces is of dimension $[1 \times 3]$, with the components distinguished between the three axis x, y, z . Only in the longitudinal equation the drag force F_d is added, moreover the rolling resistance is computed for each tire as $M_{y,ij}/r_{dyn,ij}$ and contribute to the resultant F_x . $M_{y,ij}$ is calculated with the .tir file, instead the dynamic radius $r_{dyn,ij}$ through LUTs function of vertical loads and tire pressure. As it is possible to notice the blocks are calculating the accelerations only in x, y directions. For the z axle the picture 5.7 is representing the moment equilibrium around z .

The yaw acceleration results from an equilibrium moment realised in Simulink with the cross products of the force vectors and a geometric vector. The latter gives the distance to the centre of gravity for each wheel. It also takes into account the offset of the COG on the y -axis and the z -coordinate is a function of the dynamic radius.

One of the limit of this vehicle model is due to the complexity of measuring precisely all the geometric characteristics of the car. The vehicle mass is measured during the events, but the inertia on the z -axis I_{zz} is a theoretical estimate. It is calculated at the end of the design phase, when all the members have completed the final CAD drawings for the current season. In this way, the geometries and masses of all the components are collected in an Excel file where it is possible to estimate the global inertias of the car. For the next season the team is going to validate these values through a real measurement with a Vehicle Inertia Measuring Machine VIMM, with the company CFM Schiller in Roetgen. Overall, the dual track vehicle model is a good compromise between complexity and too simplified models. The

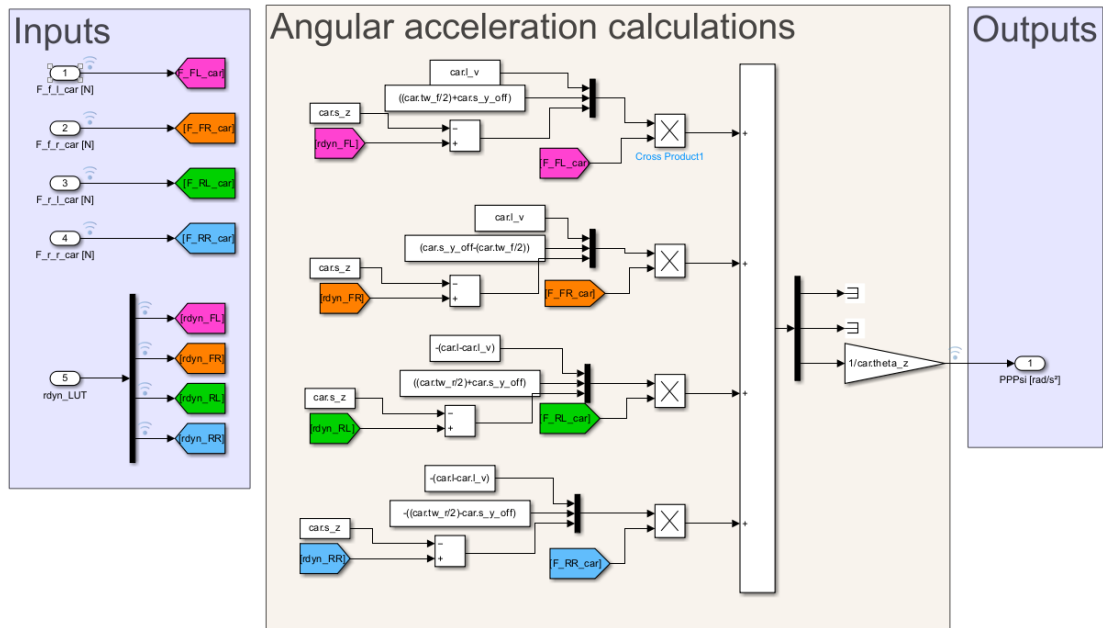


Figure 5.7: ψ equation in Simulink

goal of the thesis is the estimation of the tire parameters, for this target the 3 dof is sufficiently accurate to simulate the dynamics of the car. Moreover, the manoeuvres necessary to analyse only the lateral dynamics are relatively simple, with constant longitudinal speed of the vehicle, which makes it reasonable not to increase the complexity of the equations. The distinction between the forces of each wheel makes possible to have a better comparison with the real data.

Chapter 6

Track tests

In this chapter, an exposition of the configuration of the test tracks is presented. The initial section delineates the research methodologies employed in the identification of the manoeuvres. The subsequent segment reports the team's organisational framework and the materials utilised. Finally, an analysis of the data is conducted, with key findings illustrated through the utilisation of software vSignalizer.

6.1 Manoeuvres for testing

The test was conducted on the 9th of December at the Aldenhoven testing centre, an institution that sponsors the team Ecurie Aix. However, the timing of the test was determined well in advance, given that the centre is utilised by various customers. The primary reason for selecting this site is the periodic measurement of the friction coefficient of the asphalt throughout the year. Additionally, there is a large space available for conducting maneuvers to assess lateral behaviour.

Different papers and scientific researches have been used in order to organize the maneuvers. First reference is the paper [4] already reported in chapter 2. The authors have scheduled two sinusoidal steering strokes, a sine weave steering and a ramp steer. In the paper the first maneuver is for estimation of the parameters and the other two for validation. The sinusoidal steering stroke with a peak of 135 deg is the reference test data. Three quarters of the sine is applied and then the input is for 0,5 sec kept constant, finally the last quarter of the sine is performed. The same maneuver is repeated with the peak of 90 deg. The other two tests are done not to identify the tire parameters, but to look for results in different lateral conditions. This type of schedule is not enough for the case of study of the thesis. It is needed a larger number of tests to collect data, moreover an analysis of the transient properties of the tire is not considered in that paper. To understand deeply which maneuvers should be performed the ISO standards have been studied.

The starting point for the test methods are the ISO 7401 and ISO 4138. The international standards report the general procedure to adopt for the open loop test in lateral transient response, ISO 7401, and in steady state behavior, ISO 4138, of a road vehicle. The indications reported need to be properly adapted to the scenario of a Formula Student car. The first consideration is about the warm-up. In the ISO is reported to drive "at the test speed for a distance of 10 km or driving 500 m at 3 m/s² lateral acceleration both left and right turn." The FSAE cars have the battery capacity designed for the maximum distance of the endurance, that is 22 km. In terms of lateral acceleration, driving at 3 m/s² for 500 m is not enough to warm the tires. For these reasons the team has decided to perform 10 minutes of warm-up, stressing the tires with both right and left corners. A series of cones have been arranged in order to perform slaloms. Furthermore, the driver has utilised the given time to become more confident in their steering movements for the later manoeuvres. At the end of the time, the tire temperatures have been measured and the tire pressure is set. The selected pressure is 0.7 bar, this value comes from the experience in the past years of the team. The longitudinal speed is controlled by the Vehicle Control Unit, VCU, limiting the maximum angular speed of the motors. For each manoeuvre a different test speed is necessary, for that reason four possibilities have been defined: 20, 30, 40, 50 km/h (the corresponding engine rpm are coming from the formula: $v = rpm \cdot 2\pi \cdot r_{dyn} / 12.132 \cdot 60$, with dynamic radius 0.2 m). The main target of the track tests is to collect data to estimate the lateral forces. Moreover, to perform analysis of the transient properties of the tires, mainly to evaluate experimentally the relaxation lengths. Three manoeuvres have been performed for these reasons: ramp steer, sinusoidal sweep steer and step steering. The Step input procedure is well defined in the ISO: "Drive the vehicle at the test speed in a straight line. The initial speed shall not deviate by more than 2 km/h from the test speed. Starting from a 0 deg/s to 0,5 deg/s yaw velocity equilibrium condition, apply a steering input as rapidly as possible to a preselected value and maintain at that value for several seconds after the measured vehicle motion variables have reached a steady state. ... A steering-wheel stop may be used for selecting the input angle." [9] All the four speeds have been tested, with increasing order from 20 to 50 km/h. The maximum value of steering angle has been fixed through a series of 3D printing blocks reducing the length of the steering rack. In this way the driver is confident to reach the maximum steer in the lowest time possible. The team has developed a script that calculates the reduction of the steering rack needed to reach the target steering angle value, after that it is possible to produce the CAD for the blocks. A further check is provided by the driver display, the VCU has worked on the PCBs of the screen to provide to the driver the livetime signals of steering angle and longitudinal velocity. In this way the driver conduces the vehicle at the test speed in a straight line for the first seconds, then he applies a steering input as rapidly as possible and maintain the

command for several seconds after the measured vehicle motion variables have reached a steady state. The same maneuver is repeated several times for both right and left input. The feedback of the driver is immediately received with a bluetooth connection, without interrupting the test.

The other two maneuvers are strictly linked each other. On the ISO 7401, only the simple sinusoidal input is explained. The feedback of the Alumnis has been fundamental to organize the other part of the test. The main advantage of the sinusoidal sweep steer is the collection of a lot of information in a small amount of time. Testing at different frequencies the vehicle response is similar to perform several single sinusoidal inputs at the same time. The past experience of the Alumnis suggests the procedure to be used. The main difficulties in performing this test is the way in which the steering input has to be produced by the driver. A specific script in Matlab has been written in order to produce an audio signal that helps the driver to follow the variations of the frequencies. The audio is structured in this way: 30 seconds of silence, one sound to start the straight acceleration and reach the test speed, after 2 sec a second sound is giving the start of the steering input. Finally, a series of "beep" (different from the previous two) gives to the driver the information to change direction in the steer command. The picture 6.1 is produced by the Matlab script and it is a visual way to understand the method described.

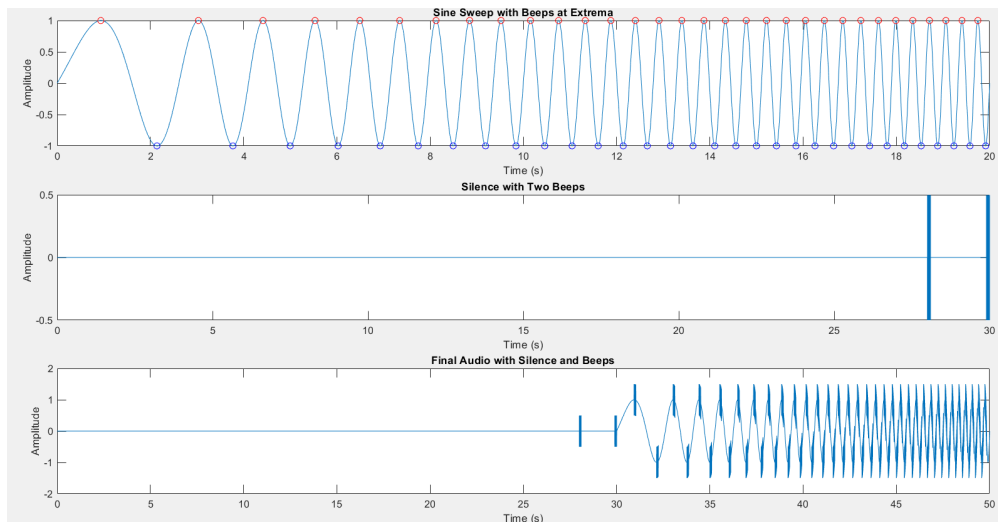


Figure 6.1: Matlab plot for the sinusoidal sweep steering audio

One audio has been produced for each test speed. In the script the starting and ending frequencies of the steering are tunable. The track experience gives as result that the driver is able to follow the sweep up to 2 Hz. The starting frequency is set equal to 0.2 Hz. Finally, the maneuver requires a total time of minimum 30 sec,

lower values will give an impossible steering command to be followed by the driver. Considering also the initial part of acceleration to reach the test speed, the sine sweep requires a very large distance. For 20 km/h about 170 m are required, for 50 km/h about 420 m. That value corresponds to the maximum that is possible to perform in the Aldenhoven circuit center. A picture 6.2 of the dynamic area of the track is reported.

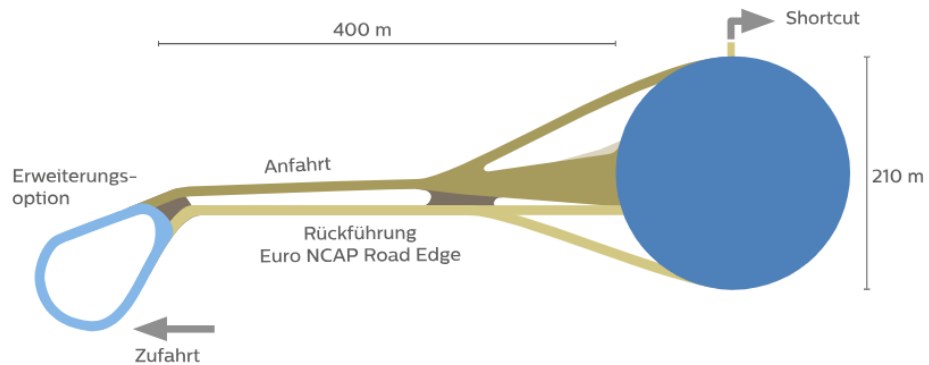


Figure 6.2: Aldenhoven testing area

The last consideration is regarding the value of the steering angle that the driver should perform as peak of the sine sweep. In order to determine it, the ISO 7401 states: "The standard steady-state lateral acceleration level is 3 m/s² or less, as necessary to remain within the range in which the vehicle exhibits linear properties. Optionally, higher lateral acceleration levels may also be used, provided the vehicle remains in the linear range."

In order to determine the value of the driver steering angle that, at the test speed, produces a lateral acceleration of 3 m/s², is necessary to perform a series of ramp steer.

These maneuvers have been performed several times for all the test speeds in both directions. After them, the logged data have been extracted to determine the target driver steering angle. This procedure has been done for 20 km/h, 30 km/h, 40 km/h. It has been asked to the driver to try to keep the same slope of the ramp and do the manoeuvre slowly keeping for some seconds the steering after the maximum rack position has been reached. Two figures 6.4 6.3 are presented for a better understanding; one coming from the real tests, the other from the paper [10].

All the studies reported in that section have been shown in a meeting with the Alumnis of the team, in order to collect important feedbacks and experiences from the past years. The advices, through "Alumni reviews", have been taken also after the tests.

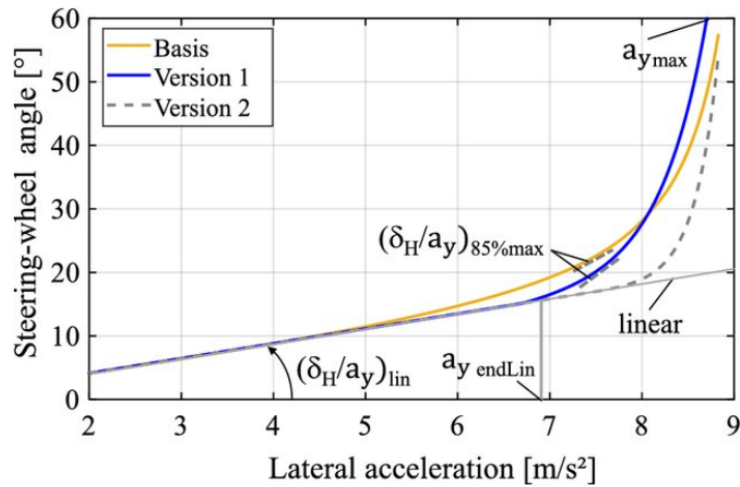


Figure 6.3: Ramp steer at 100 km/h determination of the limit of the linear range of the car, paper [10]

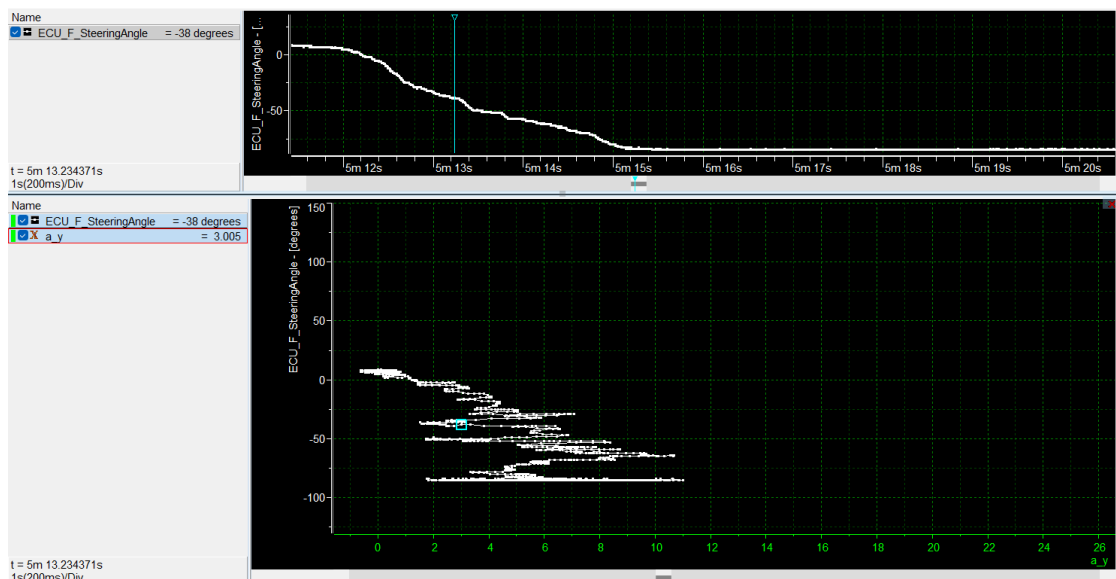


Figure 6.4: Experimental ramp data to determine the limit of the linear range of the car

Some preliminary studies have been done regarding the longitudinal dynamics manoeuvres. In this thesis they represent only a future development, the starting point is already given by the formula student team of Hamburg[11]. Some possible manoeuvres are:

- Regenerative braking: slowly braking with only rear tires. Braking with constant force on the motor, starting from a defined wheel speed for a specific interval of time (example: from wheel speed of 10 rad/s in 4 sec);
- Step: input of hard braking and then acceleration. Fluctuation of wheel speed between 10 and 12 rad/s. Constant brake force for 1 sec, then release for the next 1 sec;
- Acceleration: 8 sec of test with linear increase of F_x (tentatively because that means linear increase of a_x).

A very precise schedule has been organised, because the track was available for only 4 hours. The testing crew participated to a briefing meeting the day before, every member received a role for the following tasks: tire temperature measurement, VCU checking live telemetry and logged data, mechanics for the steering rack limitations, electrical system officer (ESO) and marshals. At the end of the day the team concluded successfully:

- Ramp steer manoeuvres: 8 runs at 40km/h, 10 at 30km/h, 9 at 20km/h;
- Sinusoidal sweep steer: 3 runs at 40km/h, 6 at 30km/h, 4 at 20km/h;
- Step steer: 2 runs at 50km/h, 6 at 40km/h, 8 at 30km/h, 7 at 20km/h;

It should be noted that not all of the scheduled tests were conducted, primarily due to adverse weather conditions that restricted the feasibility of the journey. It proved to be a near-impossible task to identify a day that met all the necessary criteria: the track was to be available, the team members were to be available to assist during the test, and the IKA Institute van was to be available. However, a more significant challenge was the prevailing weather conditions in Aachen during the winter months, which almost invariably resulted in rain. However, the driver was able to conduct a limited number of tests without freezing, due to the hard rain. The ambient temperature was approximately 2-3 °C, which made it impossible to warm up the tyres. The collected measurements reported a stable condition of 8-9 °C for the outside tyre temperature. The team tried to replicate the same test the following week, the 13th of December, not in the Aldenhven test, but in the track of the IKA institute from the RWTH University of Aachen. Unfortunately, also in that day the environmental conditions were not ideal. Immediately after the warm-up the car figured out an IMD error (Insulation Monitoring Device), that obliged the team to abort the test without collecting any data. Nevertheless, the collected data are enough to proceed with the work. In the next section an analysis of them is given.

6.2 Analysis of logged data

Ecurie Aix uses as telemetry viewer the program Vector vSignalizer. It is a simple tool to evaluate measurement data of all types. Some images from that visualizer are shown.

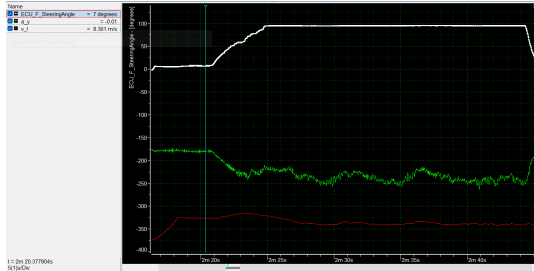


Figure 6.5: Ramp steer 30 km/h

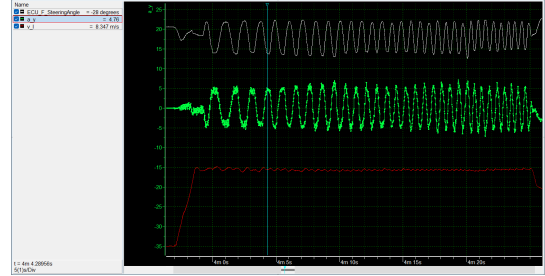


Figure 6.6: Sinusoidal sweep steer 30 km/h

In the figure 6.5 is visible a ramp steer, instead in 6.6 a sinusoidal sweep steering both performed at 30 km/h. The signals displayed are: the steering wheel angle in white, the lateral acceleration in green, the longitudinal velocity in red. Through a rough analysis is possible to appreciate how the steering locks are limiting correctly the steer amplitude, moreover also the test speed is properly kept constant at the desired value through the VCU. The vSignalizer is primarily utilised by Ecurie Aix for the purpose of rapid data analysis. However, to operate on the data, a Matlab script is employed to collect it into a struct. In this way more computations are done. The steering wheel sensor figures out an error of calibration of +7 deg, through Matlab this signal is easily corrected. The same correction is needed to the side slip angles, the formula that computes for instance the front left $\alpha_{f,l}$.

$$\alpha_{f,l} = - \left[\delta - \arctan \left(\frac{v_y + \psi l_f}{v_x - \psi \frac{b_f}{2}} \right) \right] \quad (6.1)$$

With δ steering angle at wheel level. To correct the side slip angle is necessary to add the calibration error at the previous formula (taking care of the conversion to radians and from driver to wheel reference system).

The focus should now be directed towards the sweep sinusoidal steer. It is possible to notice from vSignalizer that the driver is able to follow the increase of frequency requested. Looking at the first sine waves, the frequency evaluated in Matlab is equal to 0.69 Hz, whereas for the last waves it is 2.22 Hz. These values are sufficiently close to the theoretically requested frequencies of 0.5 Hz to 2 Hz. The analysis of the data in Matlab reveals the hysteresis of the lateral forces,

computed using the following formula:

$$F_{yF} = \frac{ma_y l_R + J_z \dot{\psi}}{l_R + l_F} \quad (6.2)$$

Where l_R and l_F are the distances of the rear and front axle to the COG, J_z moment of inertia on vertical axis, $\dot{\psi}$ yaw rate. This formulation is an approximation of the front lateral forces, it is done considering that:

- No direct sensor for the tire force is available. The best approximation that can be done is through the computation of the lateral force on the axle.
- It is considered the front axle not the rear one, because the test is conducted with only FWD. This assumes to neglect the longitudinal contribution of the force to the total front wheel force.
- The formula given is from a moment equilibrium in a bicycle model, all the limitations of this simple model hold. The load transfer is not considered in that analysis.

In the picture 6.7 the last two periods for the lateral force of a sine sweep maneuver are shown. A smaller hysteresis than desired is possible to be noticed.

This plot demonstrates that it is not possible to estimate the relaxation lengths from the data collected. This result is confirmed by the behaviour of the lateral acceleration function over time. It is also evident from the vSignalizer that the expected reduction in amplitude at high frequencies of the steering input is not present in the lateral acceleration signal 6.8.

Main reason of this result is the low longitudinal velocity of the test. The relaxation length is highly dependent on that parameter, as it is possible to appreciate in the paper [12]. The following formulation holds:

$$\tau_y \dot{F}_y^D + F_y^D = F_y^S \quad (6.3)$$

With F_y^D and F_y^S dynamic and static lateral tire forces and τ_y relaxation time, linked to the target of the relaxation length r_y through the equation:

$$\tau_y = \frac{r_y}{v_t}. \quad (6.4)$$

In which v_t is the longitudinal velocity. In the picture 6.9 is possible to see the expected behavior of the lateral force in time with a sweep sine steer. As illustrated in 6.9, the manoeuvre was executed at a velocity of 60 km/h, under constant vertical load. It is important to note that these conditions are not replicable within the test conducted in Aldenhoven. Additional factors that influence the

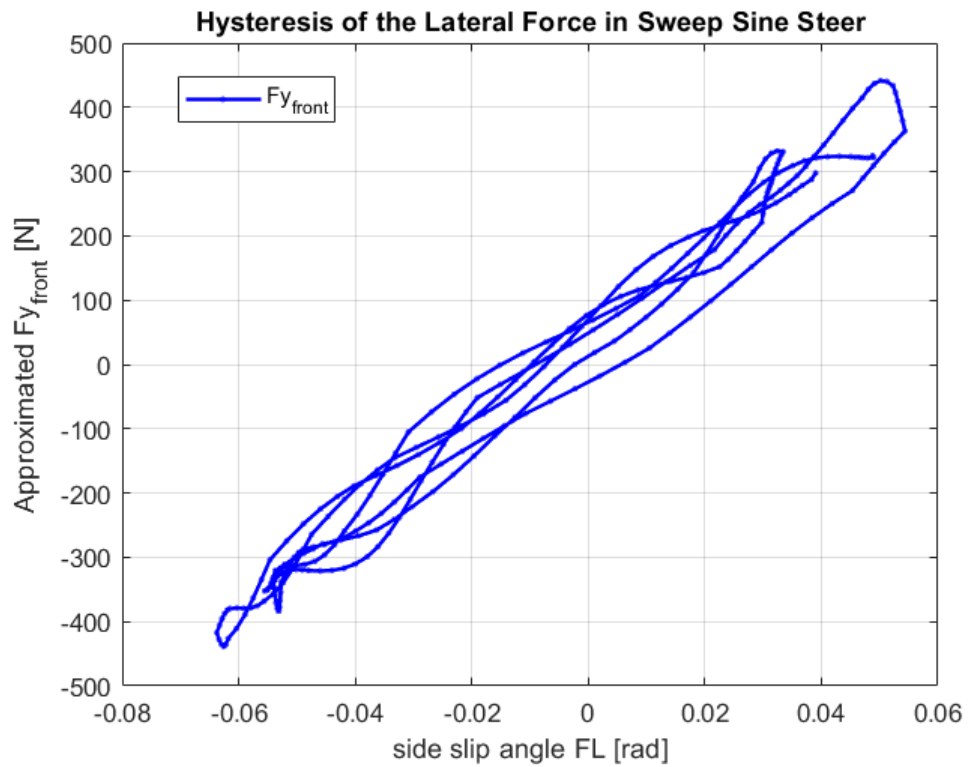


Figure 6.7: Hysteresis of lateral force in sweep sinusoidal maneuver

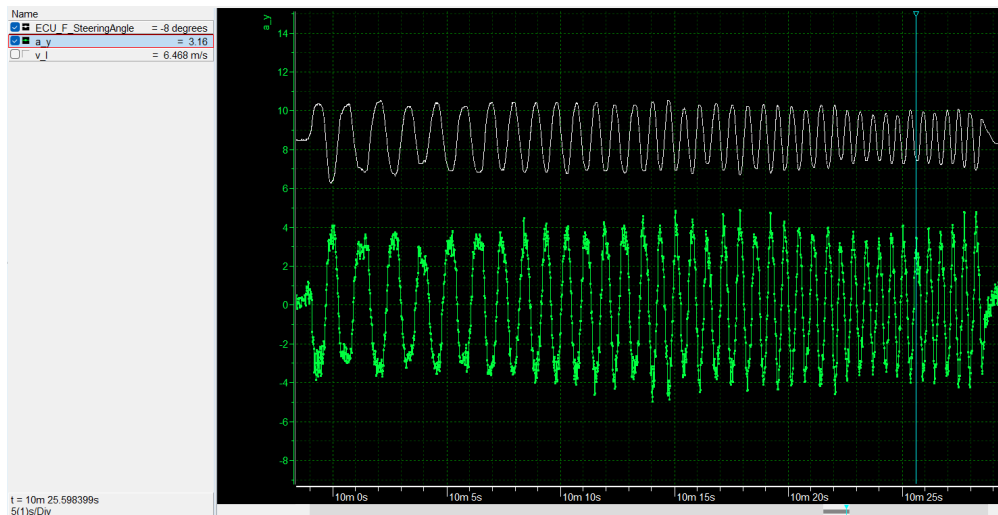


Figure 6.8: lateral acceleration and steering angle in sweep sinusoidal maneuver

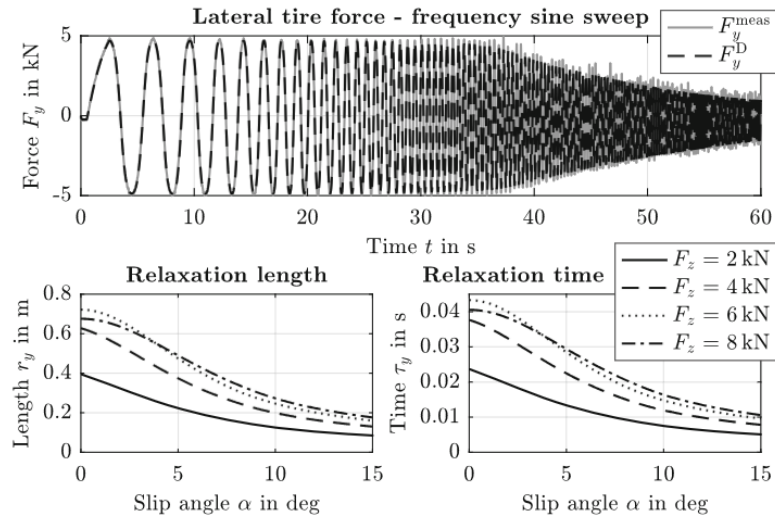


Figure 6.9: lateral force reduction in amplitude at high frequency in sweep sinusoidal maneuver

outcomes include the critical wet condition of the track and the extremely low tyre temperatures. Notwithstanding these limitations, the procedure and the work accomplished provide significant experience and a methodology for estimating the relaxation lengths. When the team replicates the test in the summer period, an estimation of these parameters will be feasible.

Focussing on the ramp steering, the runs conducted provide the data to estimate the Pacejka parameters. Following the example of the Master thesis [13] from Alexander Liniger done in the Swiss Federal Institute of Technology (ETH) Zurich, the identification can be done using slow ramp steer maneuvers. Where a slow ramp input is given to the steering angle with a slope of 0.1 rad/s, such that the steering angle does not introduce dynamic effects. That work considers the experiment in stationary conditions with $v_x = 0$, $v_y = 0$ and $\ddot{\psi} = 0$. The data from Aldenhoven are not respecting this assumptions, for that reason a deeper analysis should be done. Firstly, not all the tentatives of the ramp in the data can be used. After a selection nine ramps have been considered for the successive steps. The plots from Matlab 6.10 show the steering angle variation with time for each ramp.

From that plots the calibration error of the steering sensor is more visible. It is possible to notice that, since the car is driven by a driver, for each attempt the slope of the steering is different, moreover the time to reach the peak is between 2 sec and 4 sec. This higher slope is producing not stationary conditions, further considerations are given in the next chapter.

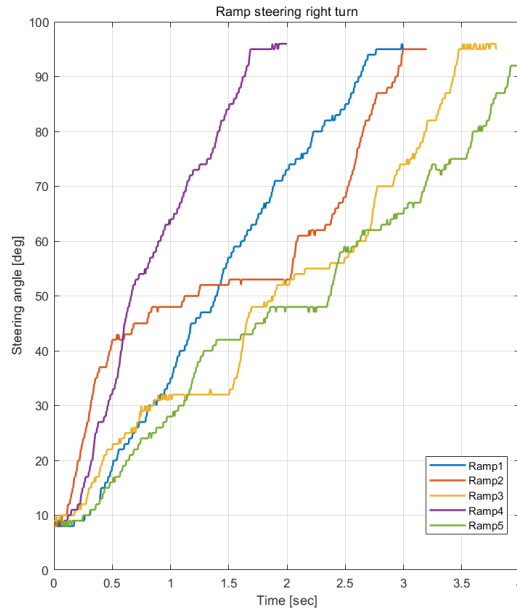


Figure 6.10: Ramp steering steering angle versus time, right turn

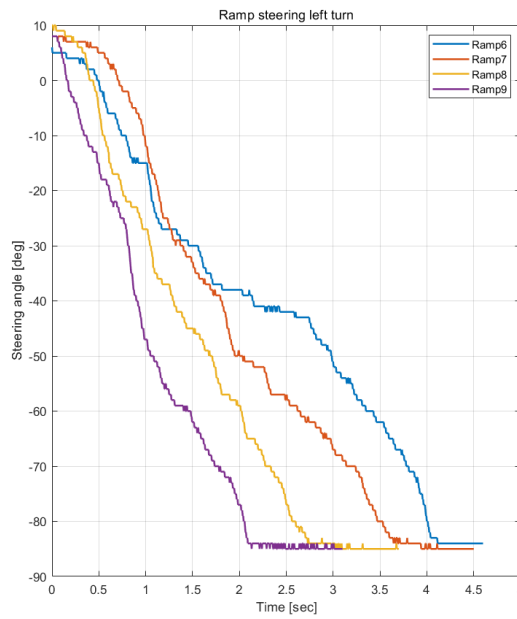


Figure 6.11: Ramp steering steering angle versus time, left turn

Chapter 7

Estimation of tire modelling parameters

In this chapter all the steps needed to obtain the tyre parameters are described. The assumptions used in the process are reported, different tyre models are investigated, finally the mathematical problem is described.

7.1 Selection of data

The first step is to select the useful data from all the logged signals. For that target only the ramps have been used as lateral maneuvers, with the characteristics already described in the chapter6. They are extracted as struct "Logdatem" in Matlab, from the complete vectors only the interesting range of time is selected. To select precisely the moment vSignalizer is used. After the definition of the time duration, the steering angle, lateral acceleration, yaw rate and side slip angle signals are extracted. For each ramp a different vector of them is created. The plot of steer angle vs time 6.10 is done to check the selected time intervals. It is worth to notice that consider more time instants after the end of the slope of the steering is giving as results more points in the saturation region of the tyre. This is possible to see directly on vSignalizer7.1, and it is mainly due to the wet and cold conditions of the tires. These environmental conditions has the advantage to show the complete evolution of the wheel force with respect to the side slip. Normally, in dry conditions the saturation of the tire force is more difficult to be detected. One of the disadvantages is that the cornering region is exploited only in half of the slope of the ramp, with a maximum of driver steering angle of about 50 deg. The physical formula used for the lateral forces has been already shown in chapter 5 6.2 and is more described in the following section. To have a proper fitting two different possibilities are developed:

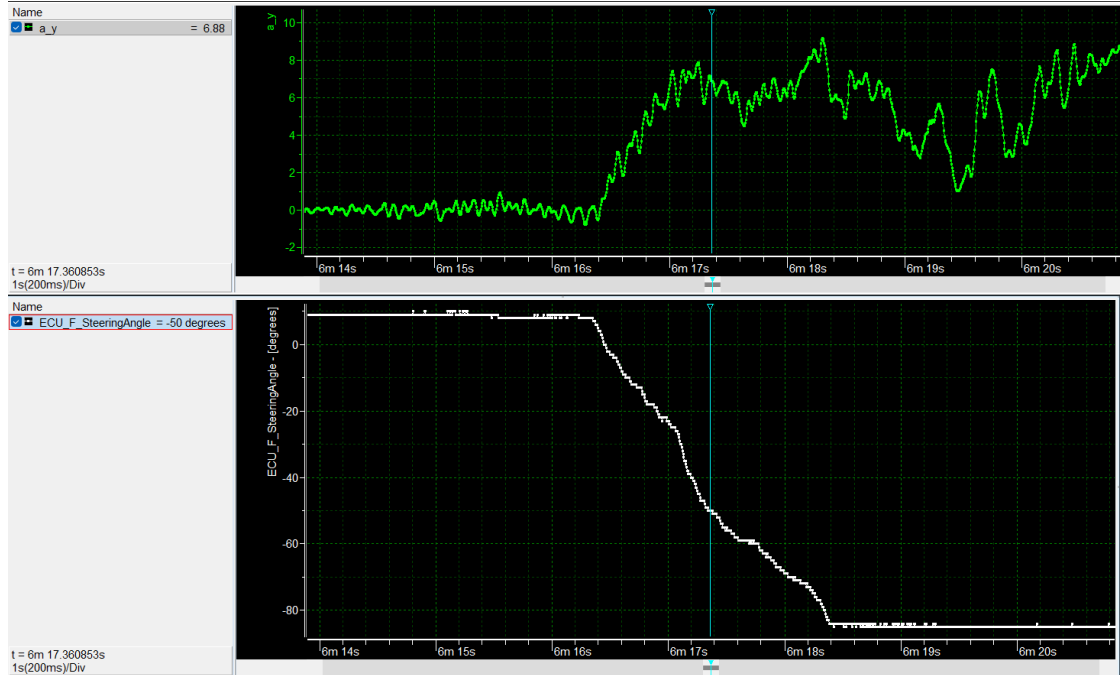


Figure 7.1: Ramp steering a_y saturation at half slope of steer angle

- Filtering of the complete ramp data in Matlab, that means postprocessing of the raw data with brushing and weighting functions;
- Extraction of the ramp data with approximately same number of points in the cornering and saturation region.

The first method consists in a postprocessing of the signals, with brushing and correction of the calibration errors of the sensors. Brush action is the remotion of very low lateral force values at high side slip angle. These come out from points at the end of the ramp slope with low lateral acceleration. The result of this process is shown in the picture 7.2, with on the left the original data and on the right the brushed ones. Final step is the centering of the data to correct the calibration of the sensors. The procedure is already described in 6.2, moreover a normalisation to the origin is performed. This is done because the initial time step is immediately before the start of the input steering. This means straight condition with zero side slip and lateral force. The final raw data are displayed in the picture 7.3, considering both ramps on left and right corners. The main drawback of this method is the excessive processing of the experimental data. The use of brushing improves the fitting, but removes experimental points without a proper physical criterion. Furthermore, this type of post-processing leads to excessive reworking of the data, all to be done manually. For a more consistent result to the experimental

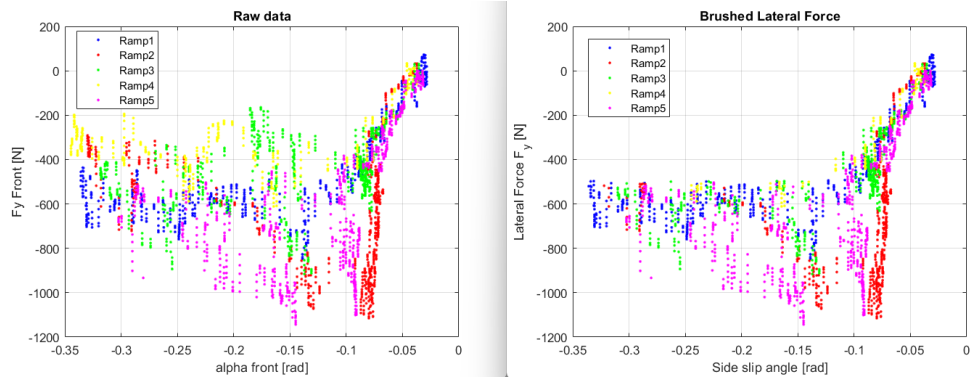


Figure 7.2: Brushing process: on the right final postprocessed data, on the left raw data

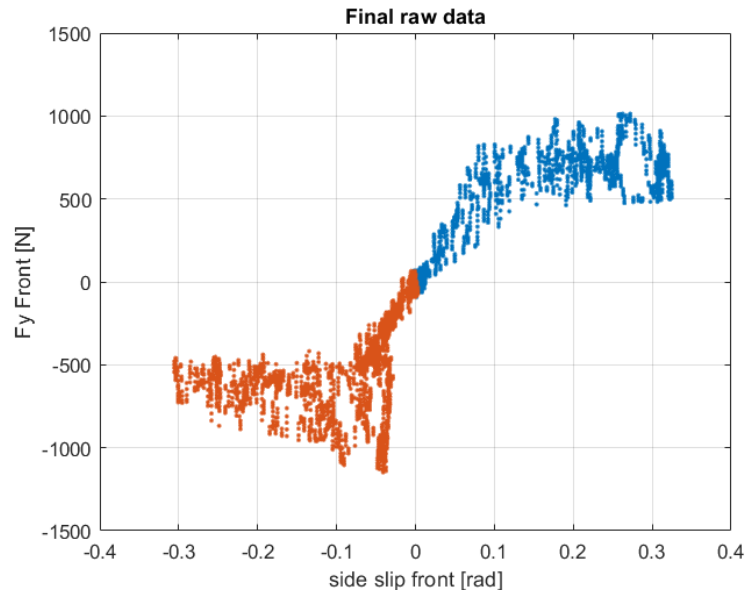


Figure 7.3: Final raw data after postprocessing with filtering (brushing and normalisation to origin)

tests, a second method is developed. An alternative to the postprocessing is the direct analysis of only part of the data. That means to extract approximately the same number of points in the cornering and saturation region of the ramp data. In order to do that, for each ramp the interval of time has been restricted, considering the behavior of the lateral acceleration visible with vSignalizer. Following the same procedure of before, the logged signals are extracted and the lateral forces evaluated. Finally, only the correction of the steering angle calibration error is applied to the side slip angle vector. No normalisation and brushing are performed,

the final set of points is displayed in the image 7.4. It is possible to appreciate an

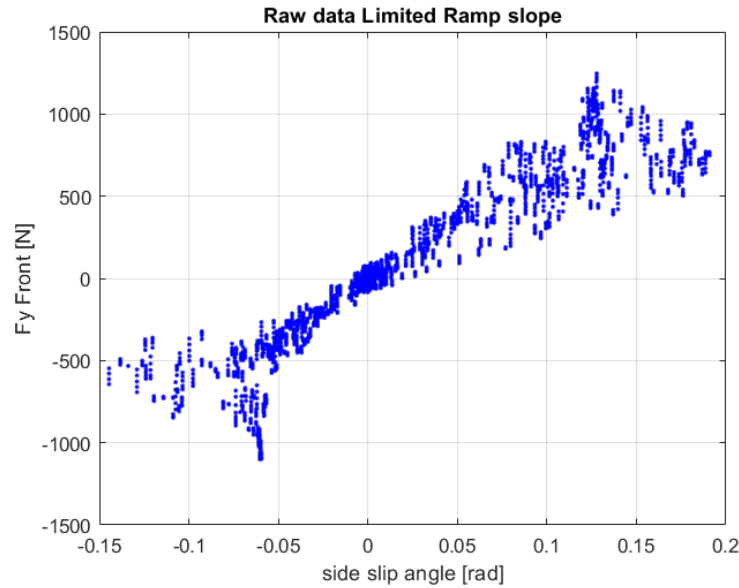


Figure 7.4: Final raw data with limited ramp slope and no postprocessing

asymmetrical behavior with respect to the origin, this result is intrinsically due to the real tests. In the positive quadrant of the axes the steering ramps have been performed for longer time, so that here the cloud of points is larger.

7.1.1 Force evaluation

The points, displayed in the pictures of the previous paragraphs, are coming out from the equilibrium of the momentum in a bicycle model. This assumption is done following the paper [14], in which the tire forces are approximated to the lateral forces computed with the lateral acceleration and the yaw rate. This approximation is necessary due to the lack of sensors. Relying only on IMU signals, the proposed formulation is the estimation closest to the real values. For the fitting procedure, a more accurate analysis is conducted considering that the tests have been done with a rear wheel drive vehicle. Normally, the formula student cars have one electric motor for each wheel. In order to reduce the longitudinal component of the tire force, the team decided to switch off the front engines. In this way, the consideration of only lateral forces exploited by the front wheels is more reliable. That problem arises always due to the lack of information regarding the wheel forces, when the longitudinal component can not be measured the best solution is

to not have its contribution.

$$F_{yF} = \frac{ma_y b + J_z \dot{\psi}}{a + b}$$

$$F_{yR} = \frac{ma_y a - J_z \dot{\psi}}{a + b}$$

With "a" and "b" front and rear axle distance to the COG, J_z moment of inertia around the z axis and $\dot{\psi}$ yaw rate. Only the front axle forces are taken into account for the fitting.

7.2 Tyre models

After the definition of the experimental set, the exploited tyre models are presented. They are reported in increasing order of complexity. Three different mathematical formulations are presented. The results of the fitting are analyzed in the next chapter. A comparison between the models is provided.

7.2.1 Simplified Pacejka

It is the first and the easier expression of the tyre forces. It takes into account the only dependence of the side slip angle.

$$F_{y,Pac} = D \cdot \sin(C \cdot \arctan(B \cdot \alpha))$$

It represents the Magic Formula, already presented in the chapter 4, with only three parameters to be evaluated. This simplified approach is also used in the reference master's thesis mentioned above [13]. The immediately next step is the introduction of the fourth parameter E:

$$F_{y,Pac} = D \cdot \sin(C \cdot \arctan(B \cdot \alpha - E \cdot (B \cdot \alpha - \arctan(B \cdot \alpha))))$$

Both the formulations are used in the following developments.

7.2.2 Normal loads

To introduce a more accurate tyre model, the dependence on the vertical forces needs to be considered. Also in that case no sensors are measuring the normal loads, for this reason they are estimated through the load transfers with logged signals of longitudinal and lateral accelerations. The used expression is the following:

$$F_{Z,FL} = m \cdot \left(\frac{l_R}{l} \cdot g - \frac{h_{CoG}}{l} \cdot a_x \right) \left(\frac{1}{2} - \frac{h_{CoG} \cdot a_y}{t_F \cdot g} \right) \quad (7.1)$$

$$F_{Z,FR} = m \cdot \left(\frac{l_R}{l} \cdot g - \frac{h_{CoG}}{l} \cdot a_x \right) \left(\frac{1}{2} + \frac{h_{CoG} \cdot a_y}{t_F \cdot g} \right) \quad (7.2)$$

$$F_{Z,RL} = m \cdot \left(\frac{l_F}{l} \cdot g + \frac{h_{CoG}}{l} \cdot a_x \right) \left(\frac{1}{2} - \frac{h_{CoG} \cdot a_y}{t_R \cdot g} \right) \quad (7.3)$$

$$F_{Z,RR} = m \cdot \left(\frac{l_F}{l} \cdot g + \frac{h_{CoG}}{l} \cdot a_x \right) \left(\frac{1}{2} + \frac{h_{CoG} \cdot a_y}{t_R \cdot g} \right) \quad (7.4)$$

With the same notation used before. The only aerodynamic contribution needs to be computed separately. The method used is the simulation through the LapSim tool of the ramp maneuvers. Through LUTs present in the Simulink, the aerodynamic load transfer is collected into a ".mat" file. The sign of the aero vertical loads is already considered in the LapTime, this leads to the simply sum of the values to the above formulas. In the figure 7.5 the behavior of F_z is displayed.

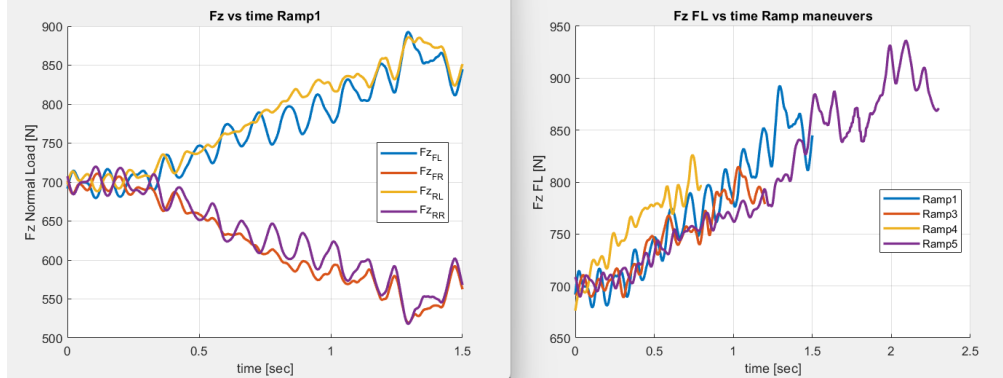


Figure 7.5: Vertical loads behavior: left picture F_z in Ramp1 for the different wheels, right picture $F_{z,FL}$ in different ramps

On the left, one single ramp is considered and the differences between the wheels are visible. On the right image, a comparison between different ramps is present. The maximum variation of vertical load is about 200 N, this means that the load transfer is not heavily affecting the dynamics of the maneuver. Nevertheless, the raw set of data, previously elaborated, can now be augmented with the vectors of F_z . For the following, the front left wheel is always considered. The 3D plot shown in 7.6 is considered as the experimental set of points through which the fitting can be done for the next models.

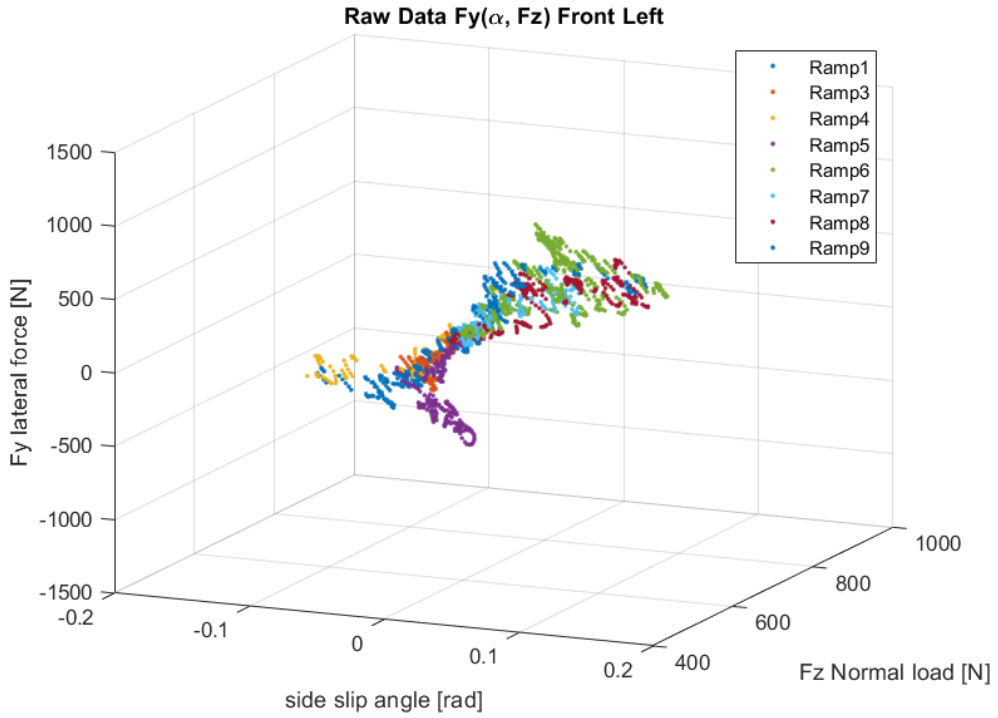


Figure 7.6: Set of raw data, plot 3D with $F_y(\alpha, F_z)$

7.2.3 Pacejka with Fz

The Pacejka tire model can now take into account not only the side slip angle but also the vertical loads. The Magic Formula takes into account of Fz through the parameter D.

$$D(\mu, F_z) = \mu \cdot F_z$$

With μ friction coefficient of the track. The problem of estimating the proper value of this variable is treated in the fitting algorithm. Due to the heavy rain conditions, a good prevision of μ is 0.6, but a range of values between [0.4, 0.7] is kept into the estimation problem. In this way the parameters to be identified are B, C and μ .

$$F_{y,Pac} = D(\mu, F_z) \cdot \sin(C \cdot \arctan(B \cdot \alpha))$$

7.2.4 Heuristic approach Kiencke and Nielsen

In the reference book [15] of Uwe Kiencke and Lars Nielsen, of the university of Karlsruhe (TH), the approximation of the tire ground contact forces is made with an adaptation of the tire slip constants. As already explained before, the linear relationship between side slip angle and lateral tire characteristics is not valid for

$a_y > 4m/s^2$ and large α . Introducing the dependence on the normal loads, the last tire model is presented. It is defined by Kiencke and Nielsen as an heuristic approach. It models the wheel forces, as function of side slip angles and normal loads, with the formula:

$$F_{y,ij} = k_{\text{red},ij} \left(k_1 - \frac{F_{z,ij}}{k_2} \right) \cdot F_{z,ij} \cdot \arctan(k_3 \cdot \alpha_{ij})$$

The reduction factor $k_{\text{red},ij}$ contains the actual friction coefficient estimation from the equation:

$$k_{\text{red},ij} = \frac{\mu_{\text{Res},ij} \cdot F_{Zij}}{\sqrt{F_{WLij}^2 + F_{WSij}^2}} \quad (7.5)$$

This factor is introduced for the reduction of the longitudinal and lateral wheel forces (F_{WLij} and F_{WSij}) ensuring that the geometrical sum of them lies in the Kamm circle. It is important for extreme driving situations, in the ramps of the thesis it is calculated but giving as result a vector of all ones values. The Kamm circle is determining the directional distribution of the friction coefficients, from them the amount of the forces. For a better understanding, the formulations used to obtain the reduction factor $k_{\text{red},ij}$ 7.5 are reported. The starting point is the wheel slip calculation. The Burckhardt approach is used. It defines the longitudinal slip s_L in the direction of the wheel ground contact point velocity $v_{W,ij}$ and the lateral slip s_s at right angles to this. The resultant wheel slip s_{res} is the geometrical sum of them.

$$s_{res} = \sqrt{s_L^2 + s_s^2}$$

With

$$s_s = \tan(\alpha)$$

The method of Burckhardt computes the resultant friction coefficient with:

$$\mu_{\text{res}}(s_{\text{res}}) = \left(c_1 \cdot \left(1 - e^{-c_2 \cdot s_{\text{res}}} \right) - c_3 s_{\text{res}} \right) \cdot e^{-c_4 \cdot s_{\text{res}} \cdot v_{\text{CoG}}} \cdot \left(1 - c_5 F_Z^2 \right) \quad (7.6)$$

This formulation is described through experimental parameters c_1, c_2, c_3, c_4, c_5 and with the resultant slip, the normal loads and the resultant speed of the COG. The parameters are reported in the book [15], distinguishing between different road characteristics. Moreover the matching between the experimental test and the estimated values is proved in the reference. For the thesis calculations, the parameters related to asphalt in wet conditions are chosen:

- $c_1 = 0.857$;
- $c_2 = 33.822$;
- $c_3 = 0.347$;

- $c_4 = 0.003 \text{ s/m}$;
- $c_5 = 0.00015 \text{ (1/kN)}^2$;

In the figure 7.7 the result from the Matlab computation of the resultant friction coefficient μ_{res} is shown. On the right, it is displayed the typical cohesion coefficient characteristics reported by Kiencke and Nielsen. The matching of the plots is confirming the good calculations. The wheel forces F_{WL} and F_{WS} are obtained

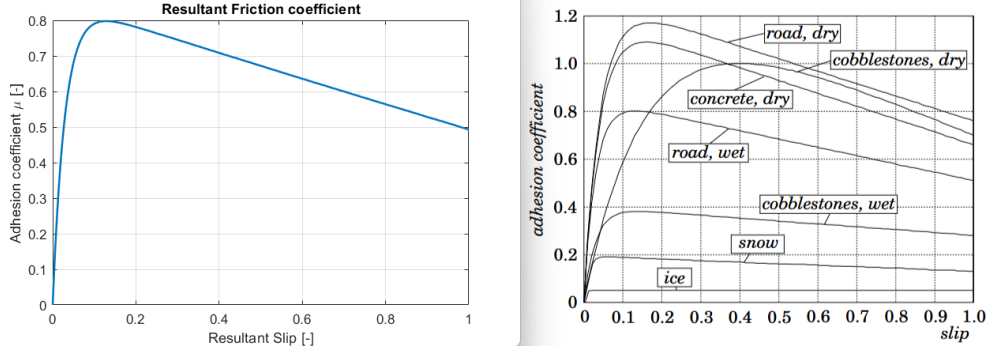


Figure 7.7: Burckhardt resultant friction coefficient: left Matlab result for Hoosier tires, right typical cohesion coefficient characteristics (Book [15] Section Vehicle Modelling p.320)

from the corresponding lateral and longitudinal friction coefficient,

$$\mu_s = k_s \mu_{res} \frac{s_s}{s_{res}}$$

and

$$\mu_L = \mu_{res} \frac{s_L}{s_{res}}$$

With k_s attenuation factor for the reduced maximum friction in lateral direction with respect to the longitudinal one.

$$F_{WL} = \mu_L F_Z = \mu_{Res} \cdot \frac{s_L}{s_{Res}} \cdot F_Z \quad (7.7)$$

$$F_{WS} = \mu_S F_Z = \mu_{Res} \cdot k_S \cdot \frac{s_S}{s_{Res}} \cdot F_Z \quad (7.8)$$

The plot 7.8, elaborated in Matlab, is showing the good behavior of the lateral force. Since the tested maneuvers are on lateral dynamics, the prevailing force is the lateral.

It emerges from the image that there is a greater concentration of points in the positive quadrant. This provides further confirmation of the preceding

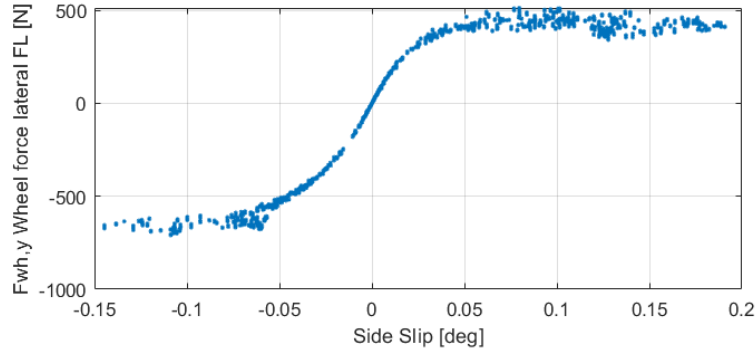


Figure 7.8: Lateral wheel force F_{WS} for front left with Kiencke and Nielsen formulation

considerations regarding the filtration of the raw data. It is also visible the saturation of the characteristics, possible to be completely seen due to the wet conditions of the track. At this point, all the quantities to evaluate the heuristic wheel forces $F_{y,ij}$ are computed. In the fitting step the tire parameters k_1 , k_2 and k_3 are determined.

7.3 Fitting procedures

In this section the mathematical problem of the fitting of the experimental data is presented. Moreover, two possible solutions are developed. The first easier approach is the use of a Matlab tool, Curve Fitter. It deals with the Levenberg-Marquardt algorithm. It has the big advantage to be userfriendly, but with some limitations. The alternative method is based on the Genetic Algorithm, whereby a dedicated script is developed, thus affording greater freedom in determining the parameters.

7.3.1 Levenberg-Marquardt algorithm

The fitting problem of a function with a set of points is based on the Least Squares Parametric Estimation. Least squares, in general, is the problem of finding a vector θ that is a local minimizer to a function that is a sum of squares, possibly subject to some constraints. A brief introduction is present in the book of Kiencke and Nielsen [15], where the mathematical formulation is given.

$$\min_{\theta} S(\theta) = \sum_{k=1}^N e^2(k) = \sum_{k=1}^N [y_p(k) - y_m(k)]^2 = \sum_{i=1}^N [F_{y,exp} - F_y(\alpha_i, \theta)]^2 \rightarrow \min \quad (7.9)$$

Where:

- y_p or $F_{y,exp}$ are the experimental observed data;
- y_m or $F_y(\alpha_i, \theta)$ are the theoretical points evaluated with the chosen mathematical tire model, parametrized with θ ;
- θ the tire parameters associated to the data y_m or $F_y(\alpha_i, \theta)$;
- $e(k)$ is the observed error;
- $S(\theta)$ is the squared error sum.

Target of the fitting is the estimation of the vector θ . The Levenberg-Marquardt algorithm (LMA) solves this problem with an iterative update of the parameters θ . A brief overview of the LMA is provided. The mathematical reasoning behind the LMA is quite involved and beyond the scope of this work. The reader is directed to references [16] for an extensive treatment. The Levenberg-Marquardt algorithm is a combination of two minimization algorithms, the gradient descent method and the Gauss-Newton method. At the beginning of the iteration the LMA acts more like a gradient descent method, then when the coefficients are close to their optimal value it acts like the Gauss-Newton method. The goodness of a fit can be measured by the total value of the sum $S(\theta)$, usually called chi-squared function χ^2 . The objective of each step is to perturb the vector θ by a quantity such that the chi-squared χ^2 is reduced. The Gradient Descent Method updates the coefficients in the downhill direction, that means in the opposite direction to the gradient of the objective function. Usually this method has a good convergence only for simple objective functions. To understand mathematically that solution, the perturbation of θ is equal to the derivative $\frac{\partial}{\partial \theta}$ of the equation 7.9. The Gauss-Newton Method presumes that the chi-squared is approximable with a quadratic function in the coefficients near the optimal solution. It uses a first-order Taylor series expansion of the objective function with the perturbation of the coefficients. Imposing to the chi-squared perturbed the $\frac{\partial \chi^2}{\partial \theta} = 0$, the update of the GNM is computed. The Levenberg-Marquardt algorithm adaptively adjusts the updated coefficients by switching between gradient descent and Gauss-Newton methods. The update of the LMA follows the equation:

$$\theta_{k+1} = \theta_k - [\mathbf{J}^T \mathbf{J} + \lambda \mathbf{I}]^{-1} \mathbf{J}^T \mathbf{r}$$

Where:

- \mathbf{J} is the Jacobian matrix, with $J_{ij} = \frac{\partial f(x_i, \theta)}{\partial \theta_j}$,
- \mathbf{r} is the residual vector, with $r_i(k) = y_p(k) - y_m(k)$,
- λ is a damping parameter to have a balance in the convergence between the Gauss-Newton algorithm (GNA) and the method of gradient descent.

When the damping coefficient λ is small, the algorithm behaves like a Gauss-Newton update, while large values of λ produce a gradient descent update. Initially, λ is set to a large value to ensure that the first updates take small steps in the steepest descent direction. If an iteration leads to a worse approximation (i.e. $\chi^2(\theta + h) > \chi^2(\theta)$), λ is increased. Conversely, as the solution improves, λ is reduced, causing the Levenberg-Marquardt method to converge towards the Gauss-Newton method, which typically speeds up convergence to the local minimum.

7.3.2 Genetic Algorithm

The second method deals with the theory of Genetic Algorithm. GA is a type of parallel heuristic search method, that means a type of search process that involves previously known information to reduce the amount of searching that needs to be done for an optimal solution. It is used in problem-solving, in that application looking to the Least Squares Problem as an optimization problem. This method for the curve fitting is widely used, since genetic algorithms have been used successfully as global optimization techniques. An example is reported in the paper of M. Gulsen [17]. The GA was originally developed for the natural selection of biological systems, from that origin come the names of the phases in which this optimization heuristic is structured. It is possible to distinguish five features: encoding, selection, crossover, mutation and culling mechanism. The encoding is a compact representation of a data structure that describes a unique solution to the problem. In the case of study, an encoding is the vector of the tire parameters that define a tyre model (for instance, B, C, D, E for the Pacejka model). The selection mechanism is the computation of the sum of the objective function, in the thesis object 7.9, that is given by the encoding. This means it takes the individual solution as input and computes the corresponding value with the objective of the optimization. The crossover mechanism produces new encodings through 'parent' encodings from the current population. In the curve fitting, that means taking new sequence of tire parameters mixing the values of previous computed solutions. The mutation phase is the perturbation of an encoding to produce a nearby solution, this mechanism is fundamental to maintain a differentiation in the pool of the population and be able to test new encodings. The last mechanism is the culling, a procedure to remove worst solutions to keep constant the size of the population. The genetic algorithm is intrinsically an iterative process, it ends only when specific criteria are reached. Scientific researches prove that GA is fairly robust and that usually it finds a near-optimal solution. This has been proven on widely different applications, the results encourage to believe that GA is able to escape local minima or maxima with the crossover and mutation mechanisms. Focussing on the thesis objective, different aspects lead to consider the genetic algorithm the best approach for the curve fitting. First of all the independence of the method to

the characteristic of the objective function. No gradient or other information are needed. Moreover, the type of search is highly parallel, with the extremely efficiency on massively parallel hardware, leading to test more combinations of parameters with the same computational time. The GA approach is viable and versatile, the tyre parameters can be restricted into a range of values. The indication of the limits in the coefficient's values is not possible to perform in the LMA. For the fitting of the tyre parameters the mathematical expressions of the function is already provided, this avoid the GA to spend time on the selection of the functional form. The knowledge of the fitting function helps in the understanding of feasible results and the limited complexity of the tyre model equations allows to have a sustainable computational effort and accurate solution. In the following the genetic algorithm is implemented in Matlab scripts through the specific "ga" function. They are divided into steps:

1. Load of experimental data: the different set of points are considered. Different fittings are performed for the filtered and brushed data and for the limited ramp steer data (as described in section 6.2).
2. Weights: definition of weight functions to increase the importance of some points in the fitting.
3. Constraints: fixed points for the final function can be defined. In the following only the origin is constrained.
4. Initial conditions of θ : the range of variation of the tyre parameters is defined. Moreover, to make the script able to run iteratively, previously computed results are assumed as new initial values.
5. Objective function and iteration: equation 7.9 is coded, the 'ga' options are defined and the iterations made.
6. Standard deviations: through the Bootstrap probability distribution, the standard deviations of the coefficients are computed.
7. Plot of the results: an image of the cloud of points, the actual and the old fitted equations are displayed. Finally, the actual parameters are stored in a ".mat" file.

In the next chapter the results are reported.

Chapter 8

Results

In this chapter the estimated tire modelling parameters are explained. Firstly, the values elaborated through the Curve Fitter Matlab tool performing the LMA are reported. Then the genetic algorithm is implemented, the tire coefficients are evaluated for the three different tyre models presented: Simplified Pacejka, Kiencke and Nielsen heuristic model, Pacejka with normal load model.

8.1 Curve Fitter with LMA

The first attempt to evaluate the parameters is made through the Matlab app Curve Fitter. This tool needs that the data points are loaded as vectors in the workspace of Matlab. The experimental data chosen are coming out from the filtering and brushing method. Then the custom fitting equation is written, the solving options are set up and automatically the result is visible as a plot 8.1. In that example the complete Magic Formula is used. The results are reported:

- $B = 16.22$;
- $C = 0.246$;
- $D = 1.698$;
- $E = -4.704$;

The standard deviations of the parameters are not computed by the Matlab app. In the plot the lateral force is expressed in kN, while the side slip in radians. It is worth noting that the fitted curve shows an unacceptable behaviour in the cornering region. The variation in the slope makes the theoretically linear region non-linear. The main reason for this is the uncontrollable range of variation of the B, C, D and E coefficients. When the Levenberg-Marquardt algorithm is used, there is no

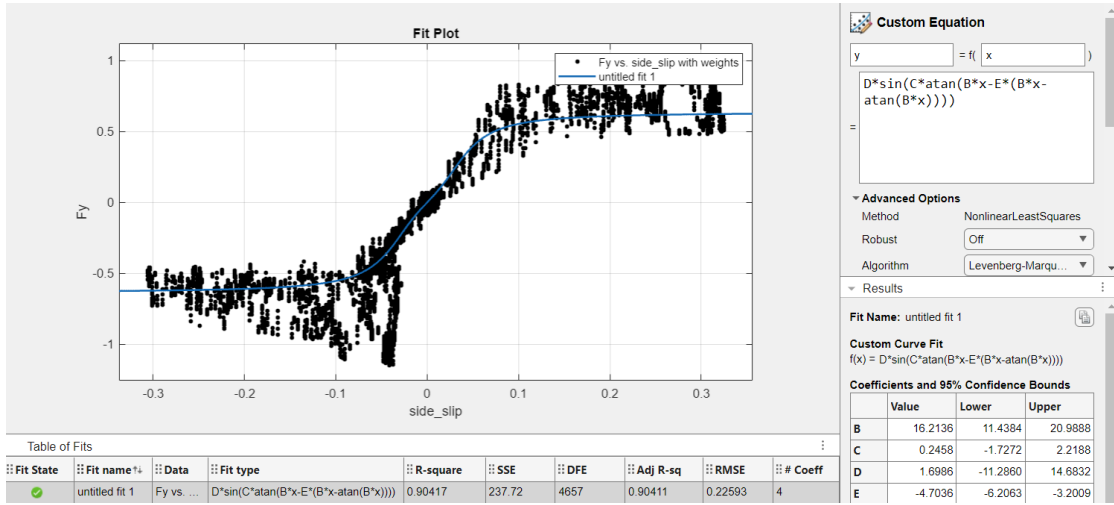


Figure 8.1: Curve Fitter Matlab with LMA

limit to the possible combinations of the parameters. This results in a sub-optimal solution. For these regions the other results rely on the genetic algorithm approach.

8.2 Lateral force characteristic $F_y(\alpha)$

The first fitting of the lateral force, through the genetic algorithm, is made with the post-processing experimental data, the ones subjected to filtering and brushing. The results are reported in the following, near the value also the standard deviation is shown:

- $B = 7.448 \pm 0.992$;
- $C = 1.745 \pm 0.138$;
- $D = 0.648 \pm 0.010$;
- $E = -0.0002 \pm 0.213$;

It is worth to notice that the last parameter E is practically zero and it changed sign considering its standard deviation. This result means that the E parameter is not useful in the fitting formula, that leads to the simplified Pacejka with only B,C and D coefficients. The Matlab script is used several times to run the genetic algorithm with initial conditions, for the tyre parameters, the previously computed value. This iterative procedure guarantee more reliable results. The first iterations of the GA have been done without weighting vectors. This leads to curves that fit better the saturated region of the tyre characteristic, but the cornering stiffness

is not matched. To give more importance to the linear region, each point in the range $[-0.5, 0.5]kN$ of the F_y have a weight equal to 10 points. In the picture 8.2 the experimental data are reported in blu, the constraint of the origin with a green circle, the curve without weighting in violet, the last fitted curve in red. The values of B, C, D and E provided before are the ones of the "Latest fitted curve".

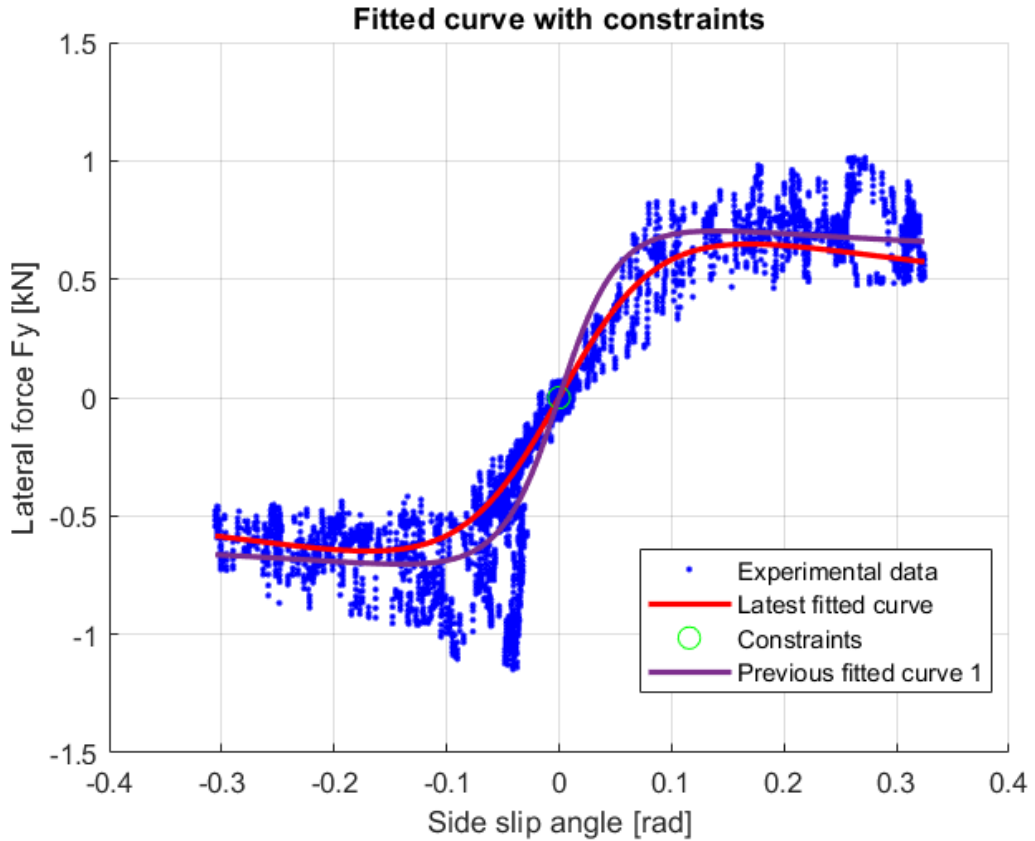


Figure 8.2: Lateral force characteristic, fitting with GA

The same procedure is repeated with the reduced ramp steer set of experimental data. As expected the new curve is fitting better the cornering stiffness region, indeed no weighting functions are necessary. The comparison between the two estimated Pacejka's characteristics is shown in the image 8.3. In blue the points of the dataset with no postprocessing, in red the new fitting curve, in green the estimation of the previous fitting with brushed experimental data. The last Pacejka parameters are:

- $B = 8.219 \pm 1.670$;
- $C = 1.360 \pm 0.555$;

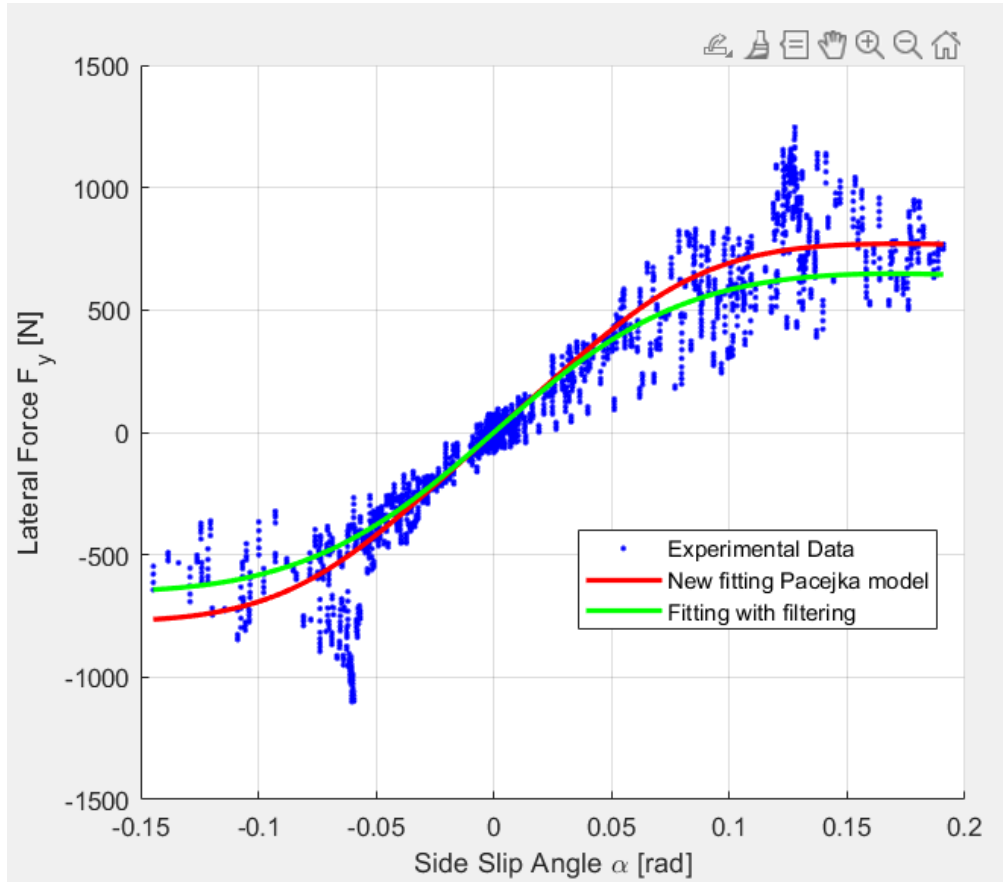


Figure 8.3: Fitting with GA: change of dataset to limited ramp steer slope

- $D = 0.771 \pm 0.011$;
- $E = -1.864 \pm 0.818$;

As it is possible to see, each parameter is not changing sign as it was with the E value in the previous results 8.2. The new coefficients and the standard deviations have proper values, confirmed by similar results in the Master thesis of Alexander Liniger from ETH [13].

8.3 Improvements on the model $F_y(\alpha, F_z)$

In this section the addition of the normal load as input in the tyre equations is considered. The first implemented model is the heuristic formula from Kiencke and

Nielsen [15].

$$F_{y,FL} = k_{\text{red},FL} \left(k_1 - \frac{F_{z,FL}}{k_2 \cdot 10^5} \right) \cdot F_{z,FL} \cdot \arctan \left[(k_3 \cdot 10^2) \cdot \alpha_{FL} \right]$$

It is worth to notice that the expected coefficients k_1 , k_2 and k_3 have not the same order of magnitude. That is the reason why in the objective function multiplication factors are present. This process take as reference the paper from Luis M. Castellanos Molina[14], in which k_1 is between 0 and 1, k_2 of the order of 10^5 and k_3 of 10^2 . This sort of normalisation in the objective function is an usefull operation for the genetic algorithm iterations. The same order of magnitude of the parameters to be estimated helps in the phase of crossover and mutation. The defined range of the parameters is: $[1, 10]$ for k_1 , $[-1, 1]$ for k_2 and $[0.1, 1]$ for k_3 . The result is shown in the picture 8.4 and the final values are here reported:

- $k_1 = 1.832 \pm 0.167$;
- $k_2 = 0.0099 \pm 0.2156$;
- $k_3 = 0.124 \pm 0.015$;

As the first fitting results, also in that case the standard deviation of k_2 is higher than the value assumed. This is probably due to the difference in the magnitude of the parameter, more trial and error should be done in order to obtain better results from this model.

The last fitting is done with the Pacejka Magic Formula taking into account the normal loads. This is done through the parameter D , for which the formulation holds:

$$D = \mu \cdot F_z$$

Where μ is the friction coefficient. Since that last variable can not be measured in the wet conditions of the track tests, two are the possibilities: assuming it constant and equal to 0.6; or considering it a variable to be estimated during the iterations of the GA. As it is possible to see by the results, the second option has been carried out taking as range of values $[0.4, 0.7]$. At the end, the value of μ is practically equal to the expected value of 0.6. The results are here listed:

- $B = 21.68 \pm 2.24$;
- $C = 1.32 \pm 0.06$;
- $\mu = 0.5986$;

In the picture 8.4 it is visible the data set with the variation of the normal loads. Since, as it has already been discussed, the load transfer in the simplified maneuvers

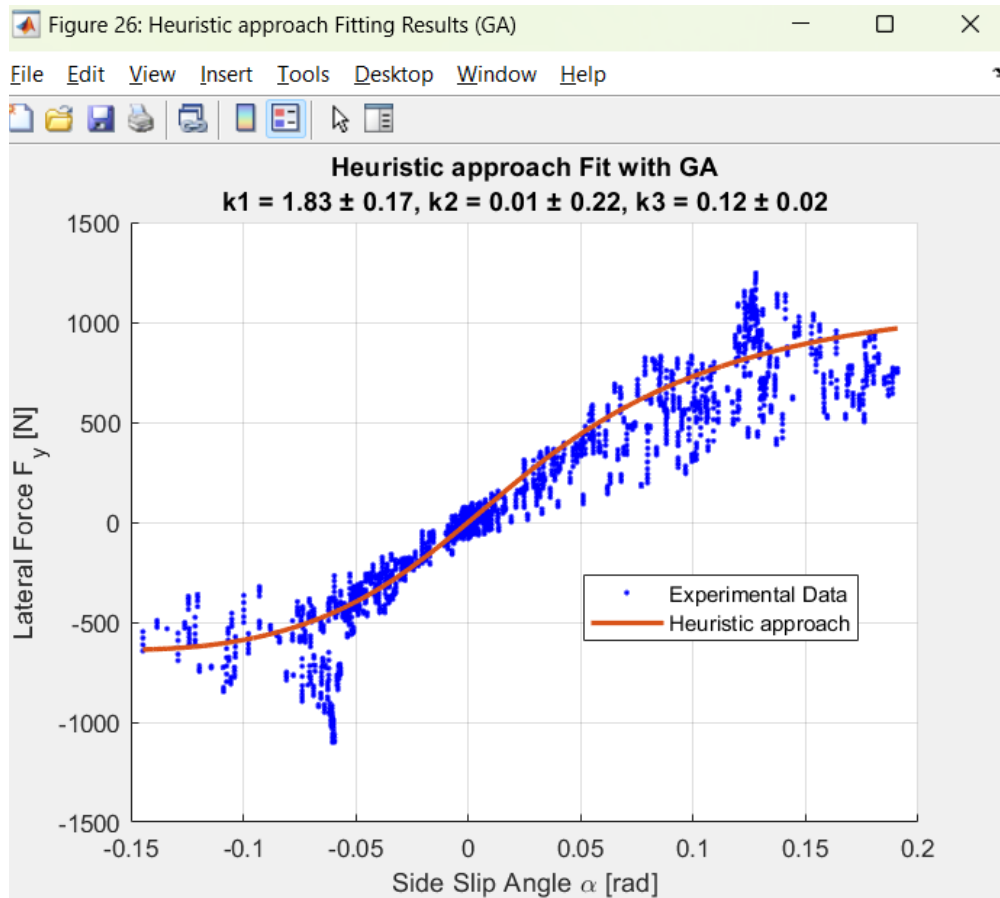


Figure 8.4: Fitting with GA: heuristic tyre model

of the test is not reaching high values, the experimental points are squeezed in a narrow variation of the F_z . This affects the fitting in the 3D view, since too few points are present for a vertical load variation analysis. Nevertheless, the tyre parameters show good standard variations and reasonable values.

A comparison between the different models is presented in the picture 8.6. The experimental data displayed in blue are coming from the not filtered ones, the red curve is the simplified Pacejka considering the GA approach, the green function is from Kiencke and Nielsen equation, the violet curve is the Pacejka Magic Formula with the parameter D function of normal loads. At first glance it may seem that the more accurate tyre model is giving the worst result in the fitting of the experimental data, the next section is explaining better this result.

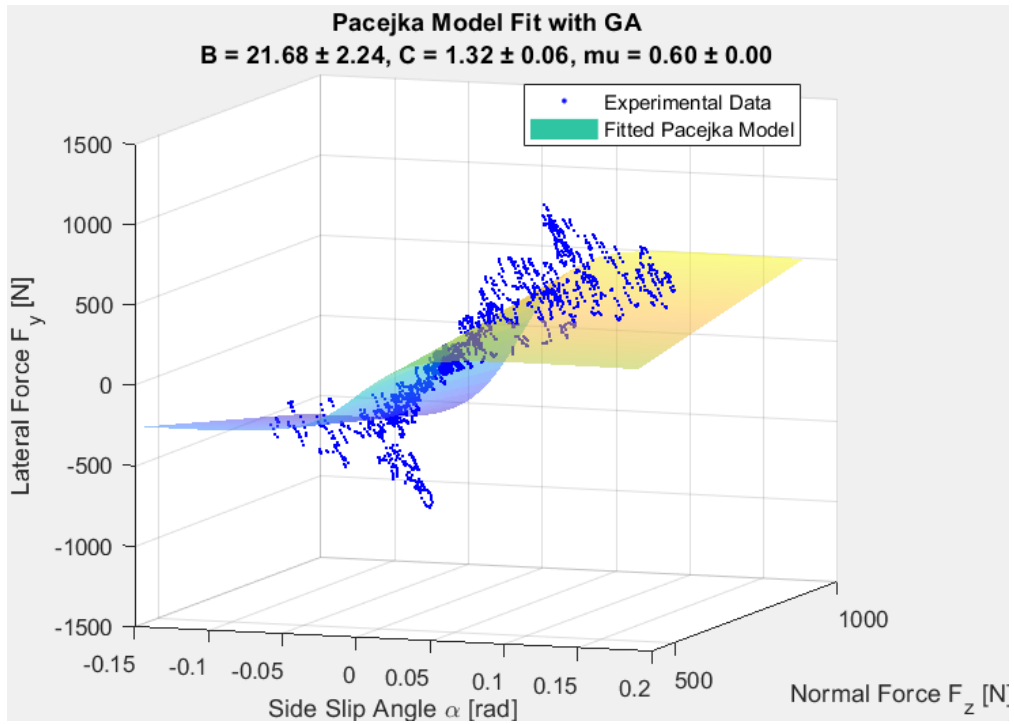


Figure 8.5: Fitting with GA: Pacejka model with F_z , 3D plot

8.4 Simulink results

To have a proper understanding of the goodness of the estimated tyre parameters, the Simulink model is used. To evaluate the lateral force of the tyre with the results, reported in the previous sections, different Matlab functions have been defined. Through a Multiport switch at each run of the Simulink it is possible to select the tyre model to use. In the Matlab functions the mathematical equations, reported in chapter 7, are implemented. 8.7

The logged lateral acceleration is compared with the simulated one. This procedure is taken as reference to understand if the tyre model, with the estimated coefficients, is giving accurate results. The maneuvers performed are the ramp steering of the experimental data set, with the configuration of the LapSim with the logged data as input. In the figure 8.8 the results of all the nine ramps are shown.

As it is possible to notice in the picture 8.8, none of the fitted models is able to follow the high fluctuations of the real lateral acceleration. The high oscillations of a_y are mainly due to the high sensitivity of the IMU, but the trend of the signal is followed by all the models. The initial values of the simulated a_y are always different from the real value. This is mainly due to the not zero value of the side slip angle

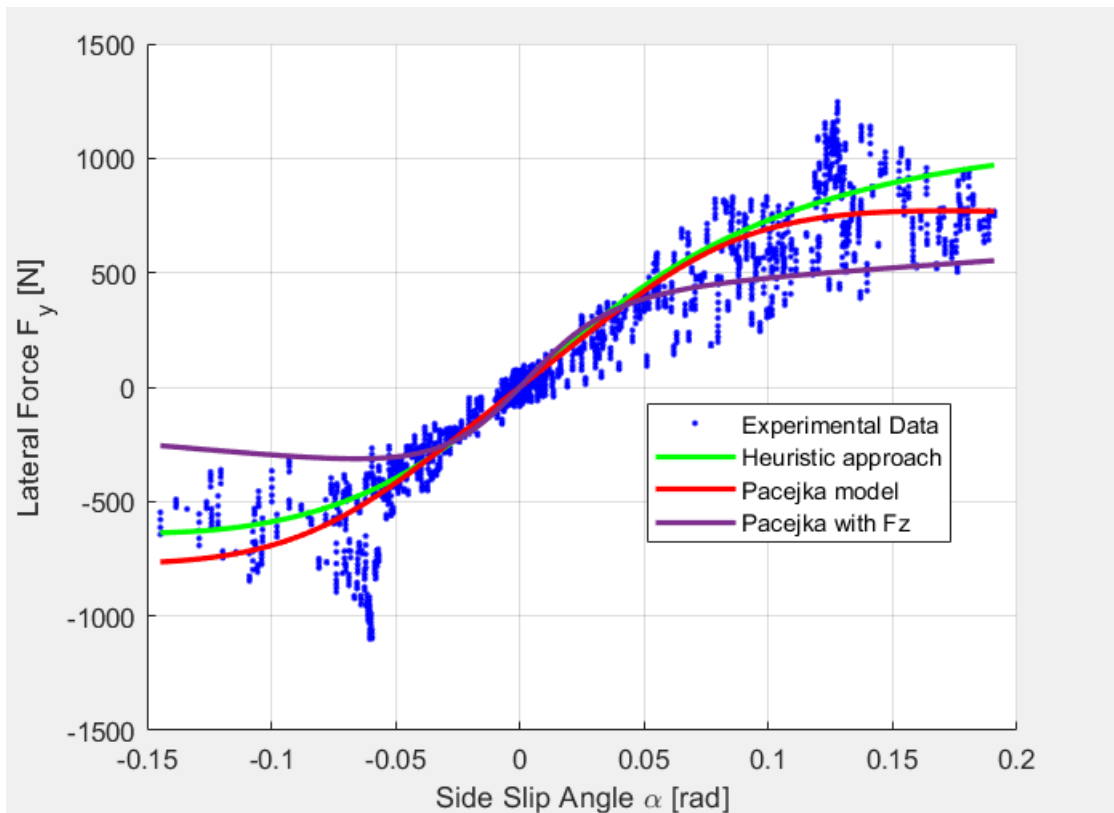


Figure 8.6: Comparison between the fitted tire models

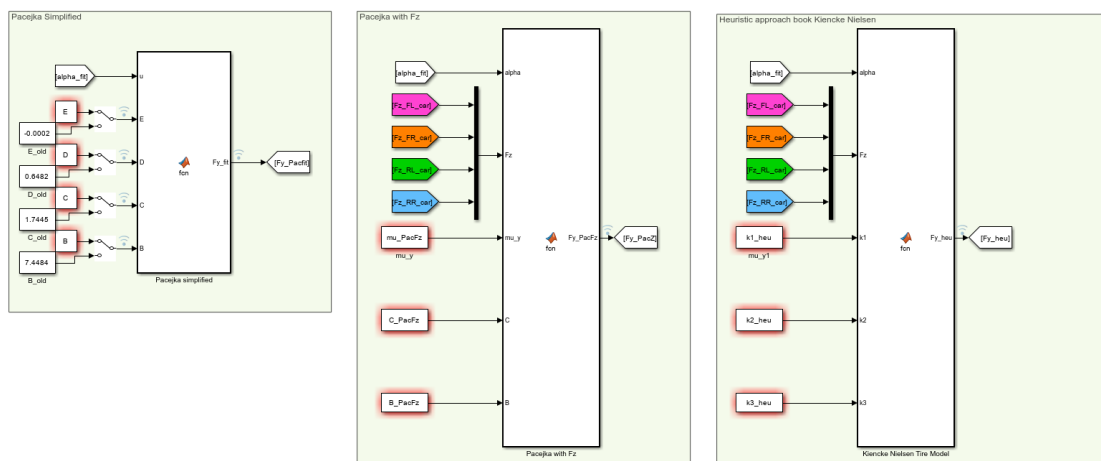


Figure 8.7: Matlab functions for the tyre models

at the beginning of the maneuver. Since the α_i vectors are coming from the logged data, even a small magnitude is giving from the equations a not zero result. Both

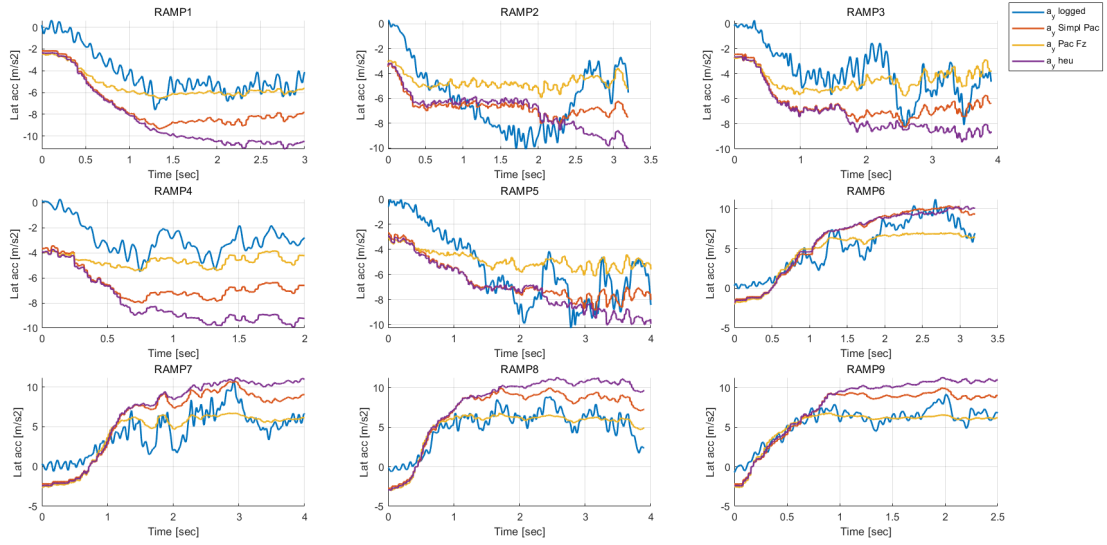


Figure 8.8: Simulated ramp steering, comparison of the fitted tire models in terms of lateral acceleration

the simplified pacejka and the heuristic approach are overestimating the lateral acceleration, in this terms the best tyre model is the Magic Formula with Fz. Even if the Pacejka model, with the contribution of the normal load, is not capable to follow the variations of the real signal, the average value of it corresponds to the logged acceleration. This result leads to consider the load transfer as an important factor in the estimation, even if it corresponds to a limited amount for this short time maneuvers. In the following the Pacejka Magic Formula with the normal loads contribution is taken as the starting model for the Extended Kalman Filter.

8.5 Extended Kalman Filter design

In order to have a simulation that is following more precisely the real behavior of the car, a control technique for a close-loop control is needed. One of the most promising methods is the use of an Extended Kalman Filter. The Kalman filter is a set of mathematical equations that provides an efficient computational (recursive) means to estimate the state of a process, in a way that minimizes the mean of the squared error. More in detail, the Kalman filter addresses the general problem of trying to estimate the state $x \in \mathbb{R}^n$ of a discrete-time controlled process that is governed by a linear stochastic difference equation. The main difference with the Extended Kalman Filter is the generalization to a non-linear process estimation function and non-linear measurement relationship to the process. This last case is of most interest and it is applied to the tire-ground contact problem. The EKF

rely on the linearization around the current estimate using the partial derivatives of the process and measurement functions to compute estimates even in the face of non-linear relationships. The non linear difference equation of the process can be written as:

$$x_k = f(x_{k-1}, u_{k-1}, w_{k-1}) \quad (8.1)$$

$$z_k = h(x_k, v_k) \quad (8.2)$$

Where f is the non-linear function that relates the state at the previous time step $k-1$ to the state at the current time step k . The non-linear function h is the measurement equation relating current state x_k to current measurement z_k . In the thesis objective the state x_k is composed by seven components.

$$x = \begin{bmatrix} v_x & v_y & \dot{\psi} & F_{y,fl} & F_{y,fr} & F_{y,rl} & F_{y,rr} \end{bmatrix} \quad (8.3)$$

Instead the input vector u_k is composed by:

$$u = \begin{bmatrix} F_{x,fl} & F_{x,fr} & F_{x,rl} & F_{x,rr} & M_{y,fl} & M_{y,fr} & M_{y,rl} & M_{y,rr} & r_{dyn,fl} & r_{dyn,fr} \\ r_{dyn,rl} & r_{dyn,rr} & \alpha_{fl} & \alpha_{fr} & \alpha_{rl} & \alpha_{rr} & & & & \end{bmatrix} \quad (8.4)$$

Finally, the measurement vector z_k or y_k is [3x1] with longitudinal, lateral velocities and yaw rate.

$$y = \begin{bmatrix} v_x & v_y & \dot{\psi} \end{bmatrix} \quad (8.5)$$

w_k and v_k are random variables that represent the process and measurement noise. They are assumed independent and white noises with Gaussian probability distribution.

$$p(w) \sim \mathcal{N}(0, Q) \quad (8.6)$$

$$p(v) \sim \mathcal{N}(0, R) \quad (8.7)$$

With Q and R covariances of the process and measurement noise. The exact value of them is not known. For the measurement covariance R it is possible to have an estimation. Repeating different off-line sample measurements of the quantities used in z_k is it possible to observe the variance of results. But the process covariance Q , since this quantities are not directly observable, is not achievable. The method that is often used is a tuning from the EKF results. It can be done through the help of another Kalman Filter performing the tuning off-line To be more precise, in the most of the cases Q and R change at each time step. In that thesis they are

assumed constant, the values are reported.

$$Q = \begin{bmatrix} 0.01 & 0 & 0 & 0 & 0 & 0 & 0 \\ 0 & 0.01 & 0 & 0 & 0 & 0 & 0 \\ 0 & 0 & 0.05 & 0 & 0 & 0 & 0 \\ 0 & 0 & 0 & 0.01 & 0 & 0 & 0 \\ 0 & 0 & 0 & 0 & 0.01 & 0 & 0 \\ 0 & 0 & 0 & 0 & 0 & 0.01 & 0 \\ 0 & 0 & 0 & 0 & 0 & 0 & 0.01 \end{bmatrix} R = \begin{bmatrix} 0.01 & 0 & 0 \\ 0 & 0.01 & 0 \\ 0 & 0 & 0.05 \end{bmatrix} \quad (8.8)$$

The values of the first three rows are related to v_x , v_y and $\dot{\psi}$ coming from the characteristics of the sensors, described in the paragraph 1.1.3. A further reference is the work presented in the bibliography [18].

The linearized governing equations can be written as.

$$x_k \approx \tilde{x}_k + A(x_{k-1} - \hat{x}_{k-1}) + Ww_{k-1} \quad (8.9)$$

$$z_k \approx \tilde{z}_k + H(x_k - \tilde{x}_k) + Vv_k \quad (8.10)$$

With \tilde{x}_k and \tilde{z}_k approximate states and measurements, \hat{x}_k a posteriori estimate. The matrixes A, W, H and V are the Jacobians of f with respect to x, w and of h with respect to x and v.

$$A_{[i,j]} = \frac{\partial f_{[i]}}{\partial x_{[j]}}(\hat{x}_{k-1}, u_{k-1}, 0) \quad (8.11)$$

$$W_{[i,j]} = \frac{\partial f_{[i]}}{\partial w_{[j]}}(\hat{x}_{k-1}, u_{k-1}, 0) \quad (8.12)$$

$$H_{[i,j]} = \frac{\partial h_{[i]}}{\partial x_{[j]}}(\tilde{x}_k, 0) \quad (8.13)$$

$$V_{[i,j]} = \frac{\partial h_{[i]}}{\partial v_{[j]}}(\tilde{x}_k, 0) \quad (8.14)$$

Applied to the thesis case of study, A is a matrix of dimension [7x7] and H [3x7]. The complete set of equations is now reported, distinguishing between time update 8.15 8.16 and measurement update equations. 8.17 8.18 8.19

$$\tilde{x}_k = f(\hat{x}_{k-1}, u_{k-1}, 0) \quad (8.15)$$

$$\tilde{P}_k = A_k P_{k-1} A_k^T + W_k Q_{k-1} W_k^T \quad (8.16)$$

$$K_k = \tilde{P}_k H_k^T (H_k \tilde{P}_k H_k^T + V_k R_k V_k^T)^{-1} \quad (8.17)$$

$$\hat{x}_k = \tilde{x}_k + K_k (z_k - h(\tilde{x}_k, 0)) \quad (8.18)$$

$$P_k = (I - K_k H_k) \tilde{P}_k \quad (8.19)$$

The equation 8.15 is the non linear difference equation already reported at the beginning of the paragraph 8.1, the only difference is the assumption of no noise w_k . The \tilde{P}_k matrix is the a priori estimate error covariance computed resolving the Difference Riccati Equation 8.16 in iterative way through the a posteriori estimate error covariance P_{k-1} . The matrix K_k in 8.17 is called Kalman predictor gain matrix, chosen to be the gain or blending factor that minimizes the a posteriori error covariance P_k in 8.19. This latter is obtained with the correction of the a priori estimate error covariance \tilde{P}_k . The equation 8.18 has the goal of finding an equation that computes an a posteriori state estimate \hat{x}_k as a linear combination of an a priori estimate \tilde{x}_k and a weighted difference between an actual measurement z_k and a measurement prediction $h(\tilde{x}_k, 0)$. This weighting is performed by the matrix K. The difference $(z_k - h(\tilde{x}_k, 0))$ is called residual or innovation.

In the figure 8.9 the complete operation of the extended Kalman filter is shown. To the reader is given the reference [19] for a deeper understanding.

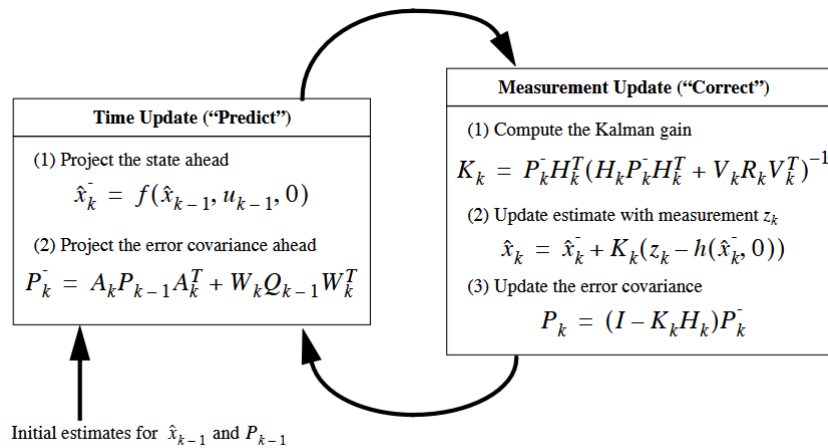


Figure 8.9: A complete picture of the operation of the extended Kalman filter [19]

The specific equations used in that thesis are now reported:

$$m \frac{d(v_x)}{dt} = F_{x_fl} + F_{x_fr} + F_{x_rl} + F_{x_rr} - \frac{M_{y_fl}}{r_{dyn_fl}} - \frac{M_{y_fr}}{r_{dyn_fr}} - \frac{M_{y_rl}}{r_{dyn_rl}} - \frac{M_{y_rr}}{r_{dyn_rr}} \quad (8.20)$$

$$m \frac{d(v_y)}{dt} = F_{y_fl} + F_{y_fr} + F_{y_rl} + F_{y_rr} \quad (8.21)$$

$$I_{zz} \frac{d(\psi)}{dt} = aF_{y_fl} - \left(\frac{t}{2} + y_{off}\right) F_{x_fl} + aF_{y_fr} - \left(\frac{t}{2} + y_{off}\right) F_{x_fr} - bF_{y_rl} + \left(\frac{t}{2} + y_{off}\right) F_{x_rl} - bF_{y_rr} - \left(\frac{t}{2} - y_{off}\right) F_{x_rr} \quad (8.22)$$

$$\frac{dF_{y_fl}}{dt} = \frac{v_x}{\sigma_{fl}} (F_{Pac_fl} - F_{y_fl}) \quad (8.23)$$

$$\frac{dF_{y_fr}}{dt} = \frac{v_x}{\sigma_{fr}} (F_{Pac_fr} - F_{y_fr}) \quad (8.24)$$

$$\frac{dF_{y_rl}}{dt} = \frac{v_x}{\sigma_{rl}} (F_{Pac_rl} - F_{y_rl}) \quad (8.25)$$

$$\frac{dF_{y_rr}}{dt} = \frac{v_x}{\sigma_{rr}} (F_{Pac_rr} - F_{y_rr}) \quad (8.26)$$

The first three equations have already described in previous paragraph 5.35.45.5, instead the last four are equal to 6.3 with assumed constant relaxation lengths σ_{ij} of 0.15 m. It is possible, starting from these equations, to compute the matrixes $A_{[i,j]}$ and $H_{[i,j]}$. The other matrixes, $W_{[i,j]}$ and $V_{[i,j]}$, are not necessary for the Simulink EKF block.

$$A = \begin{bmatrix} 1 & 0 & 0 & 0 & 0 & 0 & 0 \\ 0 & 1 & 0 & \frac{dt}{m} & \frac{dt}{m} & \frac{dt}{m} & \frac{dt}{m} \\ 0 & 0 & 1 & \frac{a \cdot dt}{I_{zz}} & \frac{a \cdot dt}{I_{zz}} & -\frac{b \cdot dt}{I_{zz}} & -\frac{b \cdot dt}{I_{zz}} \\ \frac{dt \cdot (F_{Pac_fl} - F_{y_fl})}{\sigma_{fl}} & 0 & 0 & 1 - \frac{v_x \cdot dt}{\sigma_{fl}} & 0 & 0 & 0 \\ \frac{dt \cdot (F_{Pac_fr} - F_{y_fr})}{\sigma_{fr}} & 0 & 0 & 0 & 1 - \frac{v_x \cdot dt}{\sigma_{fr}} & 0 & 0 \\ \frac{dt \cdot (F_{Pac_rl} - F_{y_rl})}{\sigma_{rl}} & 0 & 0 & 0 & 0 & 1 - \frac{v_x \cdot dt}{\sigma_{rl}} & 0 \\ \frac{dt \cdot (F_{Pac_rr} - F_{y_rr})}{\sigma_{rr}} & 0 & 0 & 0 & 0 & 0 & 1 - \frac{v_x \cdot dt}{\sigma_{rr}} \end{bmatrix} \quad (8.27)$$

$$H = \begin{bmatrix} 1 & 0 & 0 & 0 & 0 & 0 & 0 \\ 0 & 1 & 0 & 0 & 0 & 0 & 0 \\ 0 & 0 & 1 & 0 & 0 & 0 & 0 \end{bmatrix} \quad (8.28)$$

In the Simulink model the control is applied through the Extended Kalman Filter block. It requires several input: the covariances Q and R

- StateTransitionFcn: it is a Matlab function that collects the equations that hold the prediction phase of the filter. This means the time update equations. To compute the following time step of the state, it uses an Euler discretization for the derivative approximation.
- MeasurementFcn: second Matlab function, it indicates to the EKF which are the measurements to consider (v_x , v_y and yaw rate $\dot{\psi}$).
- StateTransitionJacobianFcn: third Matlab function to compute the Jacobians of the equations of the "StateTransitionFcn". In this way, at each time step, the matrixes $A_{[i,j]}$ and $W_{[i,j]}$ are updated.
- MeasurementJacobianFcn: last Matlab function, it is basically the same of the "StateTransitionJacobianFcn" but for the Jacobians of the measurement function, $H_{[i,j]}$ and $V_{[i,j]}$.
- Q and R: the covariance Matrixes for process and measurement noise.
- The states: the initial values of the states (v_x , v_y , yaw rate $\dot{\psi}$, $F_{y,fl}$, $F_{y,fr}$, $F_{y,rl}$, $F_{y,rr}$).
- StateTransitionFcnInputs: it is a Simulink signal containing all the data needed for the equations in the "StateTransitionFcn". It is the u_k vector of the equation 8.1.
- y1: it is the Simulink signal containing the vectors of the logged data used as measurements. In the case of study it is made by v_x , v_y and yaw rate $\dot{\psi}$ from logged signals, all collapsed in one vector through a mux block.

All the signals that enter in the Extended Kalman Filter Block need to be sampled, to the specific frequency 200 Hz of the IMU, starting from timeseries with a Zero-Order Hold. It is a Simulink block to keep constant the value of a signal for one time step. The LapSim modified with the Extended Kalman Filter is used to simulate the ramp steering maneuvers of the Aldenhoven track test. The results show a very accurate correction of the trend of the states. In the picture 8.10 is it possible to appreciate that the simulated signals are very close to the logged data, this emphasises the role of the EKF in the close-loop feedback correction. At the end of the maneuver, in the last instances of time, the error between the logged yaw rate and the simulated one is increasing. This means that with long simulations the convergence of the signals is not guaranteed. Since in the context of Formula Student the cornering event of Skidpad is about 4 seconds, this issue is not really relevant and not dealt in that work. Computing from v_x and v_y the lateral acceleration a_y , better results with respect to the image 8.8 are obtained. This is shown in the figures 8.11 and in the complete one 8.12. To have a closer

Results

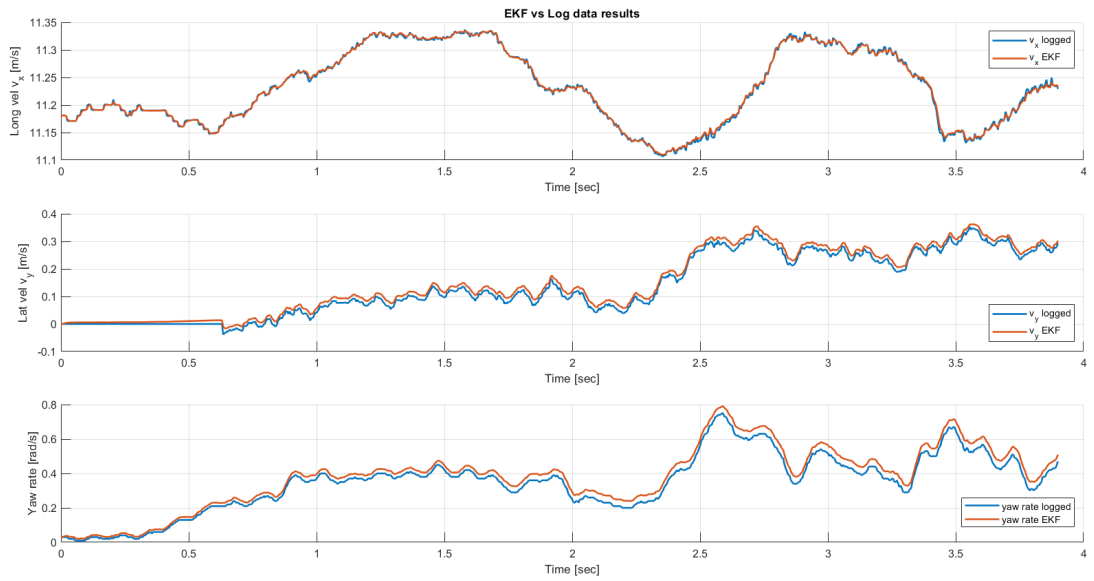


Figure 8.10: States behavior of the EKF with respect to the measurements in ramp steering simulation

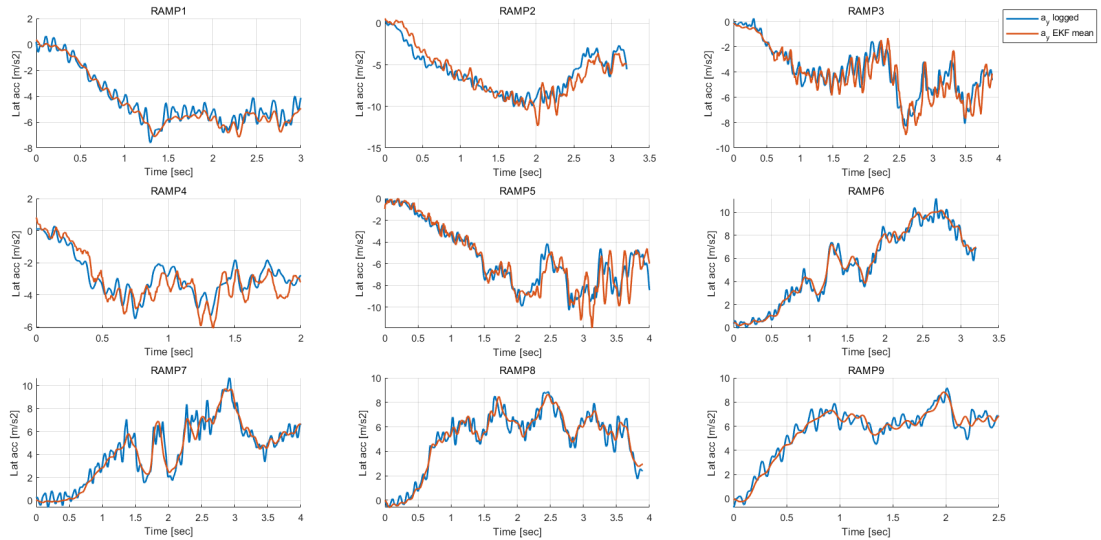


Figure 8.11: Ramp steering simulations with the signals of a_y corrected by EKF and the logged data

look a focus on the ramp3 and ramp8 is provided in the picture 8.13. The high oscillations of the logged signals are now followed by the simulated accelerations. Not a perfect match is achieved, but now the accuracy is much higher. Since the

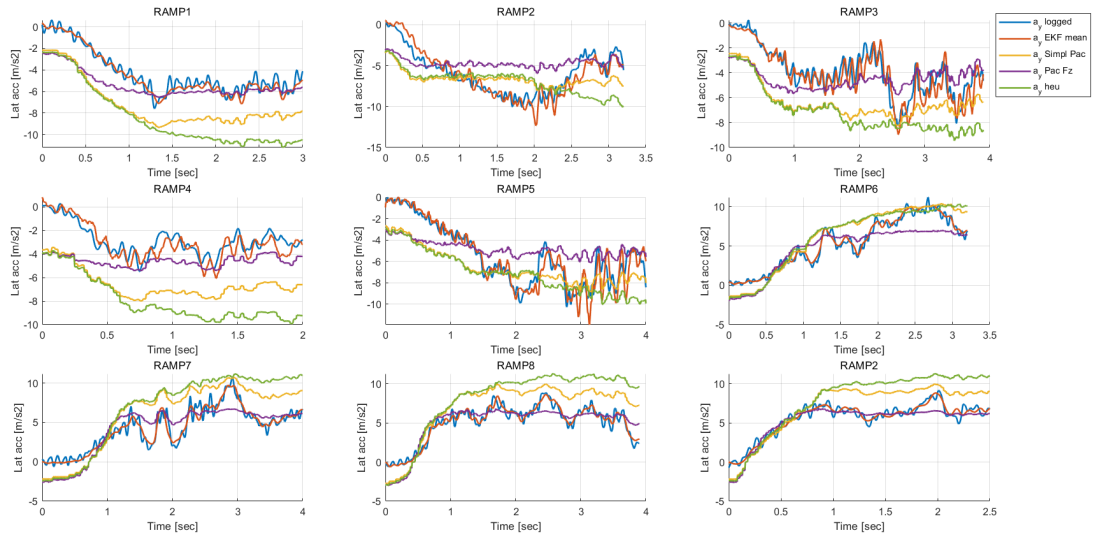


Figure 8.12: Ramp steering simulations with the signals of a_y coming from: the logged data, the tire models and the simulations corrected by EKF

targets of the simulations are the lateral forces, having the precise overlapping of logged and simulated a_y is not the priority of this work. More considerations and

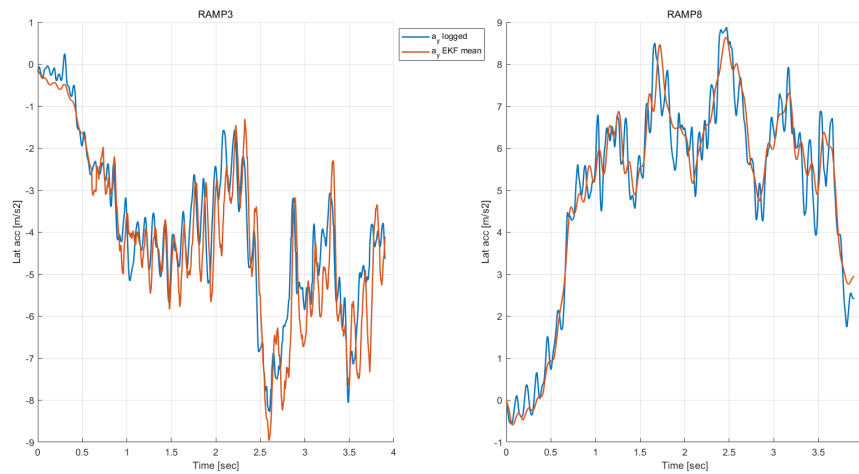


Figure 8.13: Ramp3 and Ramp8 simulations with the signals of a_y from logged data and the simulations corrected by EKF

consequences of these last results are present in the final chapter.

Chapter 9

Tire Testing Consortium Data

9.1 What is the TTC

The Formula SAE Tire Testing Consortium is the web portal mostly used by the formula student teams to analyze the tire data. The consortium works with the Calspan Tire Testing and, for the registered, teams provides all the data coming from the testing with the tire testing machine. Periodically, the TTC updates its tests providing new tested tire data, mainly based on the requests of the formula student teams. The tendency of the last years was to reduce the diameter of the wheels, that result in lower inertia, higher grip and performance. The main reason is due to the reduction of the total weight of the vehicle, this is ever years one of the goals of all the teams. Starting from more than 200 kg, the more competitive teams are now manufacturing cars of 170 kg. Ecurie Aix represents in this field one of the best formula student solutions with 162.5 kg, with the lightest battery pack of 42 kg. The reduction of the mass is affecting the vertical forces that are loading the tires. Reducing the magnitude of the static F_z and of the load transfer, lower tire diameters are able to exploit higher lateral and longitudinal forces. About five years ago the teams were practically all using pneumatics with 13 or 15 inches of diameter, nowadays most of all agree with the optimal solution of 10 inches. Every year each team tests new tires, an example of that is coming from TU Delft. From the 2021 they decided to use the tires of 8 inches. This possibilities has been considered by the other teams an excessive solution. The lack of tire data from this very small tire, the difficulty in finding these compounds and the simulated lower performances have led the teams to prefer a different tyre. A very low diameter is a strong limitation for most of the laboratory test machines, mainly due to the difficult adaptation of the sensors such as for instance the wheel force transducer

located in the rim. After some analysis and years of testing, Ecurie Aix has found in the Hoosier 43075 16x7.5-10 LCO ¹ its best compound. In this season also Hoosier 43075 16x7.5-10 R20 has been tested, a brief comparison of the laboratory data is then provided.

9.2 Laboratory data characteristics

In the web portal of the TTC there are different sections that provide not only the laboratory data, but general tire models and discussions to improve the exchange of knowledge between teams. Focussing on the data, they are structured in Rounds containing guides to explain the contents. A one-page summary of the tire/rim combination and test type for each test run is provided, in the following Run16 in Round8 for LCO and Run9 in Round9 for R20 are analysed. The selected Hoosier 43075 of 10 inches have been tested by the TTC only in lateral dynamic. This represents a bottleneck in the accuracy of the simulations. To realize the complete set of the Pacejka equations, explained in chapter 4, data from longitudinal are essential. The lack of them makes impossible to produce a ".tir" file of the tires. The solution adopted by Ecurie Aix is to scale to the 10 inches case the available data in longitudinal dynamic of the Hoosier of 13 inches with the same material. This represents the best approximation that can be done until the TTC is not publishing the requested data.

In the figure 9.1 is it possible to understand the structure of the test. Inside pressure, camber angle, normal load and side slip angle are the variables controlled by the tire testing machine. The Calspan laboratory is not controlling the tire temperature, but only storing it. The recorded variables are related to ambient temperature, road surface, tire surface center, tire surface inboard and tire surface outboard temperatures. In 9.1 the inboard surface temperature is displayed. In all cornering tests the SAE slip ratio (SL) is zero and the tire is in free-rolling condition. The primary sweeps involve varying the slip angle between ± 12 degrees for each test condition, including load, inclination and inflation pressure. The first slip angle sweep takes longer than the others because it includes several "conditioning sweeps". These serve as a final effort to prepare the tyre and ensure its performance stabilises before the main set of force and moment data is collected. The inside pressure is set at 0.55 bar and 0.84 bar, the camber angle is changed between 0, 2 and 4 degrees. The vertical force is set constant with values [222, 444, 667, 889, 1112] N. For each sweep of the side slip angle a constant set of the other parameters is tested. In the picture 9.2 the lateral force F_y is shown with respect to the different

¹Explanation of the nomenclature: 16 is total diameter in inches, 7.5 is tire width in inches, 10 is the hub diameter in inches, LCO is the material of the thread.

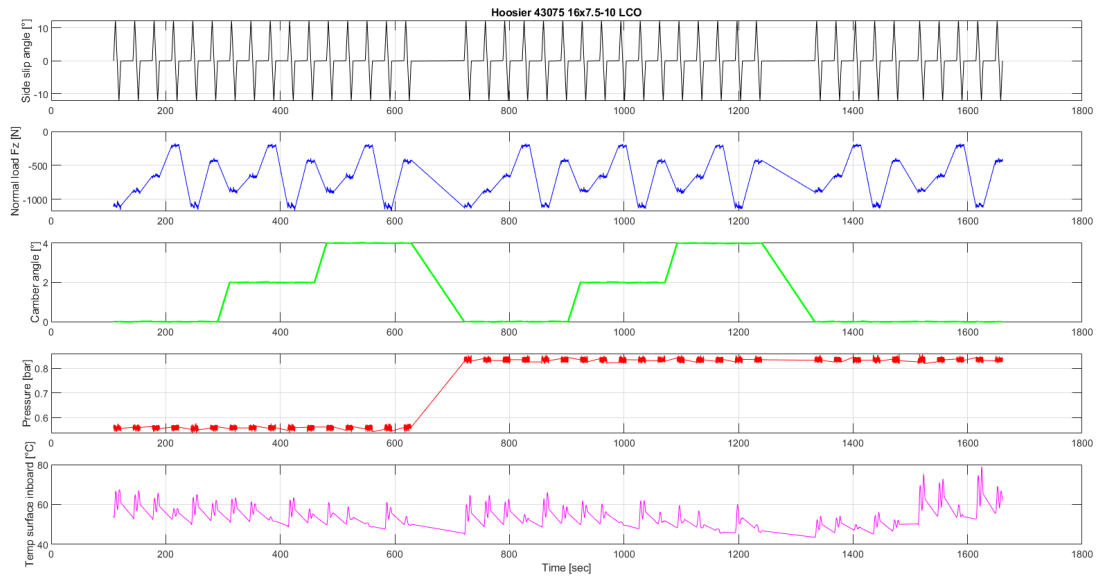


Figure 9.1: Testing cycle in lateral dynamic for Hoosier 43075 16x7.5-10 LCO from TTC

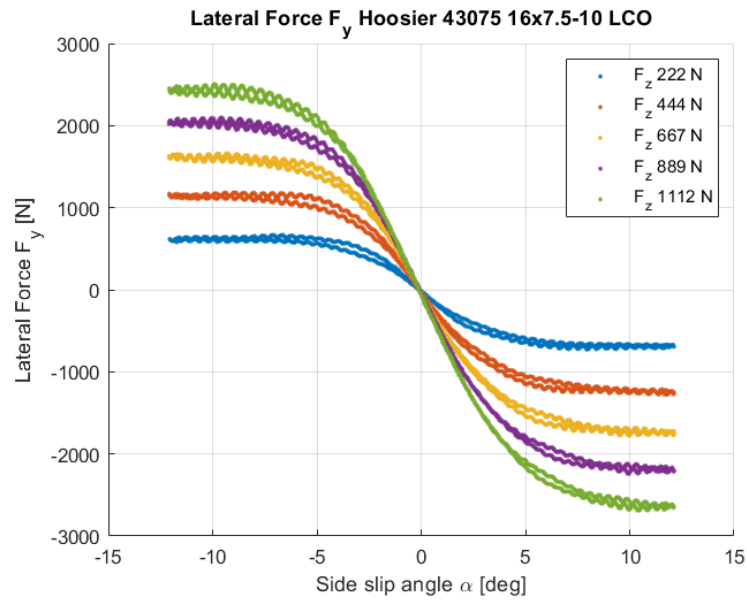


Figure 9.2: Cornering test Lateral Force F_y for Hoosier 43075 16x7.5-10 LCO from TTC

normal loads.

9.3 Comparison

It is worth to notice that with the TTC data the lateral characteristics of the Hoosier LCO and R20 can be compared. In the image 9.3 it is possible to see that

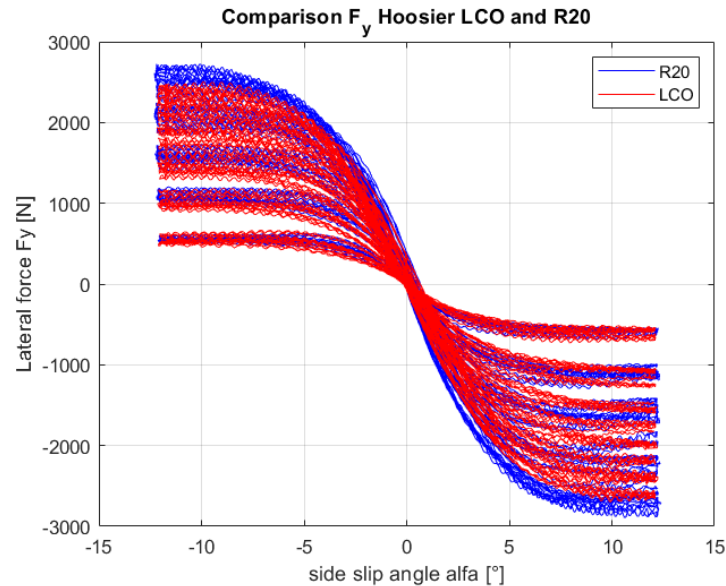


Figure 9.3: Cornering test, lateral Force F_y comparison Hoosier 43075 16x7.5-10 LCO and Hoosier 43075 16x7.5-10 R20 from TTC

at the lowest normal loads the two pneumatics provide practically the same lateral force. Increasing the vertical load the difference between the two compounds is more visible. At the highest loads, the R20 is theoretically exploiting the highest F_y . In the chapter 7.2.2 the computed range of F_z is between 500 N and 900 N, for the Ecurie Aix car. This leads to consider from the second to the last level of F_z tested by the Calspan laboratory. Taking into account this information, the team has considered the R20 as a possible improvement. As it is visible by the picture 9.3 this advantage is very small in magnitude. A further analysis has been done through real track testing. Running under the same conditions on a set up Autocross track, the team concluded that there was no difference in performance between the Hoosier LCO and the R20. More interesting analysis is done through the comparison between the experimental data of the Aldhoven test, described in chapter 6, and the TTC raw data. The teams for the thesis test has used the Hoosier LCO. Usefull data are coming from the Calspan summary table in the TTC web portal, in particular regarding the Spring Rate and Cornering Stiffness. From the laboratory the Cornering Stiffness in the 5 levels of F_z [222, 444, 667, 889, 1112] N is equal to [13.5, 20.9, 26.3, 29.6, 31.6] kN/rad. First comparison can be done

considering the estimated parameters from the Pacejka models. In the Simplified Pacejka Model the product between B, C and D that give the Cornering Stiffness is equal to 8.612 kN/rad. This very low value is mainly due to the conditions of the test. The tire temperatures were far lower with respect to the laboratory ones, moreover the wet conditions limit the performance of the pneumatic. This last different condition can be considered through a scaling factor of the friction coefficient μ . For the following comparison the notes coming from the Similarity Method in the Pacejka book [8] have been taken as reference. To compare the experimental track test data with the Tire Testing Consortium data the following formula has been used.

$$F_{y_{corrected}} = F_{y_{lab}} \frac{\mu_{road}}{\mu_{lab}} \quad (9.1)$$

The corrected F_y is the vector coming from the raw data of the laboratory, the μ_{road} is taken equal to 0.6, as already described in the chapter 8.3. Taking into account that $\mu = \frac{F_y}{F_z}$, this scaling is affecting the different vertical loads at which the tire is subjected. In the figure 9.4 the laboratory data, the experimental track test data and Pacejka fitted model are displayed in the same graph. It is worth to notice that the track data are located between the second and third level of the laboratory normal loads. They correspond to 444 N and 667 N. This range is confirming the good calculations done in section 7.2.2, where for the outside wheel in the ramp steering the normal loads varies between 450 N and 700 N.

Finally, in the last picture 9.5 it is possible to appreciate better the considerations already done. The Pacejka fitted model has a lower Cornering Stiffness with respect to the laboratory curves, but the saturation region is corresponding with the lowest loaded curve. This results are due to the discrepancies between real and laboratory environmental conditions. The saturation region is well modeled with the Pacejka due to the wet conditions that allows to detect with lot of points this phenomenon. The Cornering Stiffness region is worst represented due to cold temperatures of the tires.

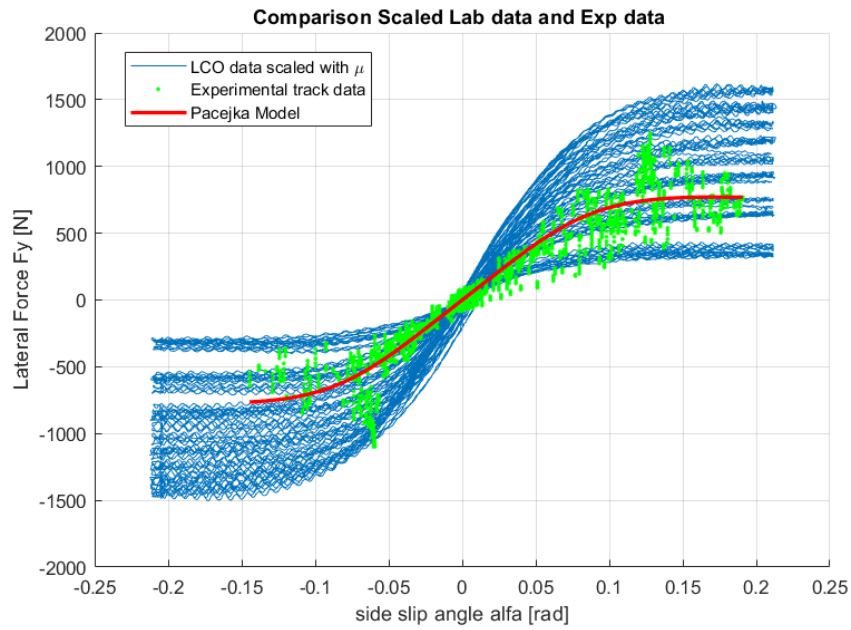


Figure 9.4: Comparison of the lateral Force F_y between TTC lab data, experimental track test data and Pacejka fitted model

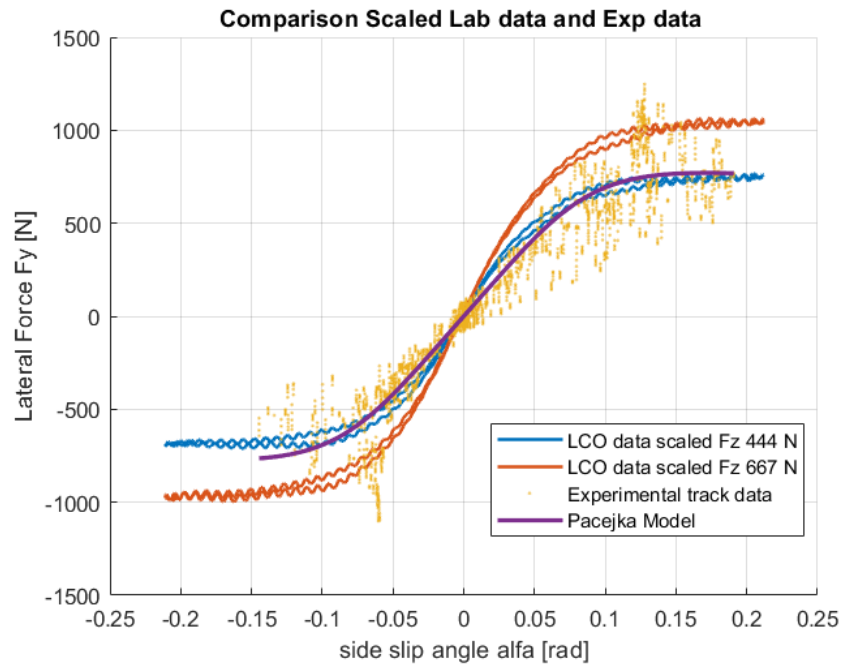


Figure 9.5: Lateral Force between TTC lab data at $F_z=444$ N and $F_z=667$ N, experimental track test data and Pacejka fitted model

Chapter 10

Conclusions

To conclude the work of the thesis it is worth to analyze the accuracies of the tire models elaborated. In order to do so, maximum and average errors have been computed for all the ramps of the track tests. The results are shown in the tables 10.1.

Mean Errors					Maximum Errors				
	Heuristic	PacejkaModel	PacejkaFz	EKF		Heuristic	PacejkaModel	PacejkaFz	EKF
Ramp1	4,141	2,978	1,224	0,406	Ramp1	6,691	4,396	3,353	1,686
Ramp2	2,485	1,970	2,116	0,889	Ramp2	6,628	4,547	5,303	4,054
Ramp3	3,294	2,505	1,559	0,642	Ramp3	7,025	5,831	3,297	3,039
Ramp4	5,118	3,715	1,771	0,593	Ramp4	7,584	5,165	4,476	1,905
Ramp5	2,070	1,632	1,938	0,676	Ramp5	4,957	3,547	4,765	3,756
Ramp6	1,540	1,477	1,451	0,371	Ramp6	4,481	4,169	4,353	1,269
Ramp7	3,350	2,608	1,407	0,533	Ramp7	7,001	5,824	3,994	2,472
Ramp8	3,434	2,391	1,002	0,431	Ramp8	7,795	5,423	3,038	1,551
Ramp9	2,768	1,909	0,731	0,434	Ramp9	6,251	4,124	2,793	1,791

Figure 10.1: Tables for averaged and maximum errors in the lateral acceleration between tire models and logged data

The Mean Errors are computed as mean value of the absolute difference between simulated a_y and logged a_y . Similar formulas are used for the Maximum Errors, in which the "max" Matlab function is used instead of the "mean". As it is possible to appreciate, the use of the Extended Kalman Filter guarantees the best results in practically all the ramps. A part from it, the Pacejka Magic Formula, with the effect of the normal loads, is showing the second lower errors. Focussing on the mean table, an average error between $1 - 2 \text{ m/s}^2$ is visible for the Pacejka model with Fz. Even if these values are low, considering the simplicity of the maneuver and the maximum values of $10 - 11 \text{ m/s}^2$ of the logged a_y , these errors are not tolerable for an accurate estimation. The max error table is showing the same behavior, in terms of goodness of the tyre models, and it emphasises the inaccuracies of the simulated a_y with the simple fitting lateral forces. The worst results are coming from the Kiencke and Nielsen tyre model. This heuristic approach is showing always an

overestimation of the lateral acceleration, as it is possible to see in the picture 8.12. All these considerations lead to strongly encourage the use of a control technique, as it is described with the Extended Kalman Filter. The development of a closed-loop feedback system has enabled the simulation to produce highly accurate results. The maximum errors visible in the table are related to spikes, in the simulated signals, that can be corrected through a moving average operation. A part from this isolated points, practically in all the ramps the a_y from EKF simulations have mean errors between $0.4 - 0.8m/s^2$. Focussing on other possible sources of inaccuracies, it is worth to notice that repeating the tests in better environmental condition could really affect the estimations. The team has already started to organize new track session in the summer period, in order to follow the procedure described by this thesis for dry track layout. An other important factor are the working conditions of the tires. With hot temperatures, higher grip is achieved and complete different scenarios can be described. This report represents the first initial step that Ecurie Aix is going to develop, in the next years, to have a deep understanding of the tyres. The methodology described can be considered as reference for the following studies. In particular, the analysis of the relaxation lengths is promising good results. All the effort put on that topic is going to give satisfaction, repeating the sinusoidal sweep maneuver as described in the chapter 6. The identification of the relaxation lengths is affecting the estimation of the tire parameters. Strong improvements for the estimation of the tyre coefficients are not expectable from the knowledge of these parameters. An higher impact is instead given by the vertical moment of inertia I_{zz} . In this work the value used is coming from CAD geometries collected by all the components of the car. This huge effort of all the team members is admirable, but it leads to strong inaccuracies. To improve this condition, Ecurie Aix has scheduled for the next year to collect data from a Vehicle Inertia Measuring Machine (VIMM), spending part of the budget for these expensive experimentally measurements. The values that are going to be collected by the VIMM are very usefull, not only for this project, but for further analysis and other divisions in the team. One of the possible next steps is to replicate the work of this thesis also for the longitudinal dynamics. In this topic, other teams have initiated the estimation of tyre parameters, especially to optimize the Acceleration event. The knowledge and the methodology developed by this thesis are again source of inspiration for that study. On the long term, the team is thinking to purchase or develop sensors to validate the estimations of the tire parameters. Possible equipments are strain gauges, wheel force trasducer WFT, accelerometers between rim and thread, as described in chapter 2. In the next testing session, the developed tool with the Extended Kalman Filter can be used to study the lateral forces developed in the Skidpad event. This is possible thanks to the accuracy of the control technique that is capable to enlarge the scenarios that are possible to be simulated. The LapSim modified, with the logged data as input, is providing information on the grip level

developed during the cornering maneuvers, typical of the Skidpad. Finally, the effects on the performance of the different set-up can be analysed in terms of tire lateral forces with the developed tool of this thesis.

Bibliography

- [1] Kistler. URL: <https://www.kistler.com/INT/en/wheel-force-transducer/C00000164> (cit. on p. 5).
- [2] Rafael A. Cordeiro. «Estimation of Vertical, Lateral, and Longitudinal Tire Forces in Four-Wheel Vehicles Using a Delayed Interconnected Cascade-Observer Structure». In: *IEEE Xplore* (2019) (cit. on pp. 5, 7).
- [3] Nan Xu Hassan Askari Yanjun Huang Jianfeng Zhou and Amir Khajepour. «Tire Force Estimation in Intelligent Tires Using Machine Learning». In: *IEEE Xplore* (2022) (cit. on p. 6).
- [4] J Kim. «Identification of lateral tyre force dynamics using an extended Kalman filter from experimental road test data». In: *Elsevier* (2008) (cit. on pp. 7, 8, 29).
- [5] Greg Welch Gary Bishop. *An introduction to Kalman Filter*. ACM, 2001 (cit. on p. 9).
- [6] Bill and Doug Milliken. *Milliken Milliken Race car vehicle dynamics*. SAE International, 1995 (cit. on pp. 10, 11, 14, 15).
- [7] Rodrigo de Oliveira Santos. *THE ABSOLUTE GUIDE TO THE RACING TYRES – PART 1: LATERAL FORCE*. URL: <http://racingcardynamics.com/racing-tires-lateral-force/> (cit. on pp. 12, 13).
- [8] Hans B. Pacejka. *Tire and Vehicle Dynamics*. Elsevier third edition, 2011 (cit. on pp. 16–18, 73).
- [9] International Organization for Standardization. *ISO 7401*. 2011 (cit. on p. 30).
- [10] Jan Sterthof Roman Henze Ferit Küçükay. «Vehicle handling improvements through Steer-by-Wire». In: *Springer* (2020) (cit. on pp. 32, 33).
- [11] e-ignition Hamburg e.V. *ARWo 2024 Identification of tire parameters using onboard sensordata by UMD Racing e.V.* (Cit. on p. 33).
- [12] Dženana Puščul Martin Schabauer Cornelia Lex. «The Influence of Transient Tire Force Transmission on Sideslip Angle Estimation». In: *ResearchGate* (2024) (cit. on p. 36).

- [13] Alexander Liniger. «Autonomous Drift Control». MA thesis. Swiss Federal Institute of Technology (ETH) Zurich, 2012 (cit. on pp. 38, 44, 56).
- [14] Luis M. Castellanos Molina Raffaele Manca Shailesh Hegde Nicola Amati Andrea Tonoli. «Predictive handling limits monitoring and agility improvement with torque vectoring on a rear in-wheel drive electric vehicle». In: *Politecnico di Torino* (2024) (cit. on pp. 43, 57).
- [15] Uwe Kiencke Lars Nielsen. *Automotive Control Systems for Engine Driveline and Vehicle*. Springer, 2005 (cit. on pp. 46–49, 57).
- [16] Henri P. Gavin. «The Levenberg-Marquardt algorithm for nonlinear least squares curve-fitting problems». In: *Duke University* (2024) (cit. on p. 50).
- [17] M. Gulsen A. E. Smith D. M. Tate. «A genetic algorithm approach to curve fitting». In: *Taylor and Francis Ltd.* (1995) (cit. on p. 51).
- [18] Adrián Blázquez Román. «Analysis and design of a lateral force estimator for a Formula Student vehicle». MA thesis. Escola Tècnica Superior d'Enginyeria Industrial de Barcelona, 2020 (cit. on p. 63).
- [19] Greg Welch Gary Bishop. *An Introduction to the Kalman Filter*. ACM University of North Carolina at Chapel Hill, 2001 (cit. on p. 64).